[45] Trangenstein, J. A., *A second order algorithm for the dynamic response of soils*, Impact Comp. Sci. Eng. 2, 1990, pp. 1–39.
[46] Trangenstein, J. A., and Pember, R. B., *The Riemann problem for longitudinal motion in an elastic-plastic bar*, SIAM J. Sci. Stat. Comput. 12, 1991, to appear.
[47] Truesdell, C., *The simplest rate theory of pure elasticity*, Comm. Pure Appl. Math. 8, 1955, pp. 123–132.
[48] Truesdell, C., and Noll, W., *The nonlinear field theories of mechanics*, in *Handbuch der Physik* 3, Springer-Verlag, 1965.
[49] Wendroff, B., *The Riemann problem for materials with nonconvex equations of state I: Isentropic flow*, J. Math. Anal. Appl. 38, 1972, pp. 454–466.
[50] Wilkins, M. L., *Calculation of elastic-plastic flow*, Meth. Comp. Phys. 3, 1964, pp. 211–263.
[51] Yee, H., *Upwind and Symmetric Shock-Capturing Schemes*, NASA Technical Memorandum 89464, NASA Ames Research Center, 1987.
[52] Zalesak, S. T., *Fully multidimensional flux corrected transport algorithms for fluids*, J. Comp. Phys. 31, 1979, p. 335.

Received November 1988.
Revised October 1989.

A Higher-Order Godunov Method for Modeling Finite Deformation in Elastic-Plastic Solids

JOHN A. TRANGENSTEIN AND PHILLIP COLELLA
Lawrence Livermore National Laboratory

Abstract

In this paper we develop a first-order system of conservation laws for finite deformation in solids, describe its characteristic structure, and use this analysis to develop a second-order numerical method for problems involving finite deformation and plasticity. The equations of mass, momentum, and energy conservation in Lagrangian and Eulerian frames of reference are combined with kinetic equations of state for the stress and with caloric equations of state for the internal energy, as well as with auxiliary equations representing equality of mixed partial derivatives of the deformation gradient. Particular attention is paid to the influence of a curl constraint on the deformation gradient, so that the characteristic speeds transform properly between the two frames of reference. Next, we consider models in rate-form for isotropic elastic-plastic materials with work-hardening, and examine the circumstances under which these models lead to hyperbolic systems for the equations of motion. In spite of the fact that these models violate thermodynamic principles in such a way that the acoustic tensor becomes nonsymmetric, we still find that the characteristic speeds are always real for elastic behavior, and essentially always real for plastic response. These results allow us to construct a second-order Godunov method for the computation of three-dimensional displacement in a one-dimensional material viewed in the Lagrangian frame of reference. We also describe a technique for the approximate solution of Riemann problems in order to determine numerical fluxes in this algorithm. Finally, we present numerical examples of the results of the algorithm.

1. Introduction

1.1. Overview

Solids often exhibit nonlinear behavior under sufficient applied forces. Materials may stiffen or soften as they are compressed, leading to a nonlinear relation between the material restoring forces and the deformation. This nonlinear deformation is elastic if the material returns to its original shape when the applied force is removed. In other cases the deformation is plastic, meaning that permanent dislocations of the constitutive chemical bonds or particle positions have occurred. Another source of nonlinear response in materials is due to the geometry of large deformations. These nonlinear material effects can be important in a variety of physical problems. In this paper, we are interested in the dynamic response of nonlinear materials, especially due to large forces such as earthquakes and explosions.

Our goal is to develop numerical methods for the computation of propagating discontinuities in nonlinear solids. Since second-order Godunov methods were successful when applied to problems involving local linear degeneracies and complicated global wave structure in petroleum reservoir simulation (see [6], [42], [43]), we have decided to develop second-order Godunov methods for finite deformation in elastic-plastic solids. This necessitates some analytical development for solid mechanics: the equations of motion must be formulated as a first-order system, and

Communications on Pure and Applied Mathematics, Vol. XLIV, 41–100 (1991)
 CCC 0010-3640/91/010041-60$04.00

the local hyperbolic structure of this system must be determined. We apply this analysis to several material models of practical interest, and examine the circumstances under which these models lead to hyperbolic systems for the equations of motion. This work constitutes the first principal result of this paper. The second principal result is the development of the second-order Godunov method for finite-deformation in elastic-plastic solids for general constitutive laws, even those given in rate form. This numerical method then provides a useful tool for beginning a study of waves in elastic-plastic solids, both in this paper and other papers to follow.

The equations of motion for general continua are derived from laws describing the conservation of mass, momentum, and energy. In the Lagrangian frame of reference, these laws take the form

$$0 = \frac{\partial \rho_L}{\partial \tau},$$

$$\rho_L f^T = \frac{\partial \rho_L \mathbf{v}^T}{\partial \tau} - \nabla_a^T (S_L F^T), \tag{1.1}$$

$$\rho_L(\omega + f^T \mathbf{v}) = \frac{\partial \rho_L(\epsilon + \frac{1}{2}\mathbf{v}^T\mathbf{v})}{\partial \tau} - \nabla_a^T (s_L F^T \mathbf{v}).$$

Here ρ_L is the mass per volume at rest, τ is time, f is the vector of body forces per mass, v is the vector of particle velocities, a is the vector Lagrangian spatial coordinates, S_L is the second Piola-Kirchhoff stress tensor, $F = \partial x/\partial a$ is the gradient of the current particle position, ω is the radiative heat transfer per mass, and ϵ is the internal energy per mass. In three dimensions, there is one equation for conservation of mass, three equations for conservation of momentum, and one more equation for conservation of energy, for a total of five conservation equations. However, these equations involve twenty-one unknowns: density, velocity, stress (which is a symmetric 3×3 matrix), deformation gradient F, temperature and internal energy. In order to close the system, we must specify sixteen additional relationships among these unknowns, so that the end result is a first-order hyperbolic system.

Two different types of equations are needed to close the system. The first type consists of constitutive laws that characterize the material. For example, in an elastic material the stress tensor is related to the deformation gradient by a kinetic equation of state. Of course, there are many other kinds of constitutive equations of use in modeling solid mechanics. Since our ultimate purpose is to identify a general form for use with our analysis of the equations of motion, we have chosen the rate-form

$$\frac{dFS_L e_i}{d\tau} = \mathbf{H}_{ij} \frac{dFe_j}{d\tau} + \mathbf{h}_i \frac{d\theta}{d\tau} \tag{1.2}$$

for our characteristic analysis, since it includes a large class of constitutive models currently in use. (In Section 4 below we discuss how other models, not given in rate-form, can be treated with our analysis.) Here, θ is the absolute temperature and e_i is the unit vector in the i-th coordinate direction. Of course, we assume that the parameters $\mathbf{H}_{ij}$ and $\mathbf{h}_i$ in this equation satisfy the constraint that this equation of state is invariant under rotations of the frame of reference. In addition to the kinetic equation of state, we also relate the internal energy to the temperature and possibly the deformation gradient by a caloric equation of state.

Note that because (1.2) is an ordinary differential equation, it allows the stress to depend on the history of the deformation gradient and temperature. Because this evolution equation for stress cannot be written in conservation form, this means that our system of equations is not, strictly speaking, a system of conservation laws. As a result, the jumps across discontinuities could in principle be dependent on the internal structure of the discontinuity.

The other type of equation needed to close the system of equations is some identity relating the deformation gradient to the velocity. In the Lagrangian frame of reference, this identity takes the form

$$\frac{dF}{d\tau} = \frac{\partial \mathbf{v}}{\partial a}. \tag{1.3}$$

Here are nine equations that can be added to the seven equations from the constitutive models to obtain a closed system of Lagrangian equations, with all but the ordinary differential equations (1.2) for the constitutive laws in conservation form. In addition, we assume that the initial-value constraint

$$\nabla_a \times F^T = 0 \tag{1.4}$$

is satisfied by the deformation gradient; if this constraint is satisfied initially, then (1.3) shows that it is satisfied for all time.

In the Eulerian frame of reference, there is a delicate point regarding the form of the equality of mixed partials. An identity analogous to (1.3) can be obtained by the Implicit Function Theorem:

$$\frac{\partial F^{-1}}{\partial \tau} = -\frac{\partial F^{-1}\mathbf{v}}{\partial x}. \tag{1.5}$$

However, a direct characteristic analysis of the resulting first-order system leads to characteristic speeds that are not properly analogous to the Lagrangian speeds, and to spurious eigenvector deficiencies. In a numerical scheme, such anomalies could have disastrous consequences. These difficulties can be overcome by using another identity for equality of mixed partials,

$$\nabla_x \times F^{-T} = 0, \tag{1.6}$$

in order to rewrite (1.5) in the non-conservation form

$$\frac{dF^{-1}}{d\tau} = -F^{-1}\frac{\partial v}{\partial x}. \tag{1.7}$$

The system of partial differential equations involving (1.7) and the Eulerian form of (1.1), with the Eulerian form of (1.2) to provide information about partial derivatives of stress, has characteristic speeds that are properly related to the Lagrangian speeds. The constraint (1.6) is also an initial value constraint.

In Section 5 below, we collect the physical conservation laws, constitutive laws, and auxiliary identities into closed systems of differential equations for both frames of reference. Specifically, we show that the Lagrangian characteristic speeds are either zero, or occur in plus/minus pairs corresponding to the square roots of the eigenvalues of the 3×3 Lagrangian acoustic tensor. The Eulerian characteristic speeds are related to the Lagrangian speeds by

$$\lambda_E = n_E^T v + \lambda_L \| F^T n_E \|.$$

An eigenvector deficiency occurs if one of the plus/minus pairs of Lagrangian characteristic speeds is zero (or, equivalently, if one of the analogous Eulerian wavespeeds is equal to the normal velocity). Furthermore, the characteristic directions for either of the full systems of conservation laws can be easily obtained from the eigenvectors of the corresponding acoustic tensor.

Once the general analysis of the characteristic structure of the equations of motion has been established, the next task is to apply the analysis to specific constitutive models. We consider three-dimensional finite deformation of isotropic models using the Jaumann stress rate, and elastic-plastic models with work-hardening. In the elastic case, the acoustic tensor is

$$A = H + C,$$

where

$$H = I\frac{\mu}{\rho_E} + n_E \frac{\kappa + \frac{\mu}{3}}{\rho_E} n_E^T,$$

$$C = [I n_E^T S_E n_E + S_E n_E n_E^T - n_E n_E^T S_E - S_E]\frac{1}{2\rho_E}.$$

Here n_E is the direction of propagation in physical space, S_E is the Cauchy stress tensor, and ρ_E is the mass per volume in the current configuration. The symmetric matrix H is positive-definite, with eigenvalues equal to the squares of the standard p- and s-wave speeds of isotropic linearly elastic infinitesimal displacement. The nonsymmetric matrix C is due to the form used by the Jaumann stress rate to guarantee rotational invariance. In spite of the nonsymmetry, we show that this matrix C is such that the acoustic tensor has real eigenvalues, which are positive provided that the difference between the largest and smallest principal stresses is not too large.

During plastic response, the acoustic tensor takes the form

$$A = H - m\frac{1}{\beta}m^T + C.$$

Because this matrix is a rank-one symmetric perturbation of the previous acoustic tensor, the characteristic speeds during plastic response cannot be larger than those in elastic response. Our analysis shows that plastic yielding causes a discontinuous decrease in the characteristic speeds from those obtained in elastic response, and as a result it is possible to see more than one wave in the same wave family. It also appears to be possible to obtain complex characteristic speeds with these models if the yield strength is sufficiently large; however, the yield strength is generally fairly low, and as a result we have not yet observed complex wavespeeds for elastic-plastic response in metals.

Given the analysis discussed above, we have the analytic information required to formulate a second-order Godunov method; see [6]. This algorithm is described in Section 7 below. In this method, we use the characteristic form of the equations to compute fluxes, which are differenced conservatively. Second-order accuracy in smooth regions is obtained by constructing piecewise linear interpolants as initial data for the characteristic solution at each time step, and oscillations at discontinuities are suppressed by limiting the characteristic amplitudes of these interpolants. The ordinary differential equation (1.2) is integrated subject to yield constraints in order to update the stress in a rotationally invariant fashion. In the present work, we consider three-dimensional displacements in a one-dimensional material; this allows us to study both compressional and shear waves while simplifying the numerical method for this initial work. We have also limited the method in this paper to the Lagrangian frame of reference, for two reasons. First, the approximate solution of the Riemann problem is less difficult in the Lagrangian frame than in the Eulerian frame. Second, it is trivial to find the initial conditions for integrating the stress-rate equations along particle paths in the Lagrangian frame.

In the eighth section of the paper we present numerical results to verify the analysis and the method. The examples involve finite deformation of a nonlinear elastic-plastic metal undergoing various levels of compression, tension, and shear. As expected, the Godunov method is able to resolve strong shocks without developing destructive oscillations or excessive smearing of discontinuities and clipping of peaks. We observe a variety of nonlinear wave behavior in the various regimes tested, including compound waves due to local linear degeneracies in the characteristic structure. In compressions we find that the elastic precursor shock and the plastic shock are both in the same wave family and are separated by a constant state that has associated with it a discontinuous change in characteristic speed. This

behavior is due to the fact that states on the yield surface have two characteristic speeds associated with them, depending on whether the material response is elastic or plastic. In a second set of examples, we compare the numerical results from the second-order Godunov method to the analytic solution for spherical wave propagation in solids with pressurized inner cavities. Here the numerical results do not show any of the oscillations commonly produced by standard finite difference or finite element methods, and the time lag between the pressure rise and the peak response is small.

Even though our numerical method only uses information about the local wave structure, it is still possible to solve problems with complicated global wave structure. Our numerical results show convergence to solutions involving, for example, local linear degeneracies, partly as a result of our conservative difference scheme and judicious use of numerical viscosity.

1.2. Previous Analyses

The characteristic structure of the equations of motion in elastic solids has been studied by a number of authors. Truesdell and Noll in [47] examined the conditions for real characteristic speeds in isothermal isotropic elastic solids and related those conditions to the S-E (strongly elliptic) condition; an analysis of thermoelastic solids can be found in [1]. A number of authors (who were surveyed well in [27]) studied the shock jump conditions in various frames of reference for abstract constitutive laws. Cristescu in [11] considered a variety of applications in solid mechanics, from vibrating strings and membranes to solids described in a conservative Eulerian framework. He examined the jump conditions for shocks, but avoided a discussion of analytical or numerical results for problems involving complications due to coincident characteristic speeds (i.e., loss of strict hyperbolicity) or to the existence of extrema of the characteristic speeds along the individual wave curves (i.e., local linear degeneracies).

In recent years, the structure of solutions to problems involving local linear degeneracies or loss of strict hyperbolicity has been addressed by several mathematicians. Wendroff (see [48]) constructed the global solution to Riemann problems for strictly hyperbolic systems with local linear degeneracies or linearly degenerate waves, and Liu (see [29]) proved the existence of these solutions. They found that the individual wave curves could involve compound waves consisting of rarefactions and shocks. Keyfitz and Kranzer (see [25]) examined Cristescu's model for a vibrating string and constructed the solution to the Riemann problem in terms of strains and velocities. In this model, the square of one of the characteristic speeds is the derivative of the tension with respect to the strain, while the other speed squared is the tension divided by the deformation gradient. Thus it is possible for the two characteristic speeds to be equal at one or more values of the strain, with a coincidence of the wave characteristics. As a result, the solution of the Riemann problem is more complicated than for strictly hyperbolic systems. Recently, Tang and Ting (see [41]) examined the characteristic structure of general one-dimensional deformation of nonlinear elastic solids. Unlike Keyfitz and Kranzer, Tang and Ting inverted the stress-strain relationship and examined the interaction of waves in

terms of the components of the stress tensor. They found that the characteristic speeds can become equal at umbilic points, around which the structure of the solution of Riemann problems is quite complicated. Unfortunately, the work by Tang and Ting does not generalize to many of the most-commonly-used material models, because the stress-strain relationships for these models are not invertible. In passing, we note that additional work on the structure of solutions to general hyperbolic 2×2 systems is under study by Shearer in [38]; also, there is work by Shearer in [39] and Holden in [19] to determine the structure of the solutions to systems with finite elliptic regions, such as occur in strain-softening materials or materials with non-convex strain energy functionals.

1.3. Other Numerical Methods

The standard numerical approach for computing the dynamic response of solids has been to solve the equations of motion in non-conservation form using centered differences coupled with additional artificial viscosity. There is a significant disadvantage to this approach. In order to guarantee stability of the scheme and convergence to the entropy-satisfying solution of the equations of motion, an appropriate amount of artificial viscosity must be added. Typically, it is impractical to add enough artificial viscosity to suppress all of the oscillations, since this smears discontinuities too much. These oscillations are a cause of significant concern in problems involving elastic-plastic solids, since they can lead to unphysical ratcheting of the material response alternately on and off the yield surface. One could consider using flux-corrected transport (see [8], [51]) to control the introduction of artificial viscosity, but this method has been known to produce entropy-violating discontinuities for conservation laws with local linear degeneracies.

Another approach that has been receiving increasing attention by the engineering and mathematical communities in recent years is streamline diffusion (see [21], [23]). This method has provable convergence properties for problems in which a transformation to "entropy variables" is available, so that the selection of the physically meaningful solution to the equations of motion is natural. However, the entropy variables for general constitutive models in solid mechanics are unknown; as a result, some analytical work still needs to be done to guarantee the convergence of this method to the physically realistic solution for problems involving strong shocks.

2. Notation

The notation of solid mechanics is by no means standardized; as a result, we have adopted conventions that are particularly well-adapted to the use of linear algebra in the characteristic analysis below. We shall denote scalars by lower-case Greek letters, vectors by lower-case Roman letters, and matrices by upper-case (Greek and Roman) letters. Somewhat in contradiction of this convention, we shall retain the same lower-case character for the entries of vectors and upper-case letters for the entries of matrices. Vectors will always be understood to be "column vectors." Also, we shall use summation conventions when convenient.

As an example, the vector a will be written

$$a = \begin{bmatrix} a_1 \\ a_2 \\ a_3 \end{bmatrix}.$$

The gradient with respect to a is

$$\nabla_a = \begin{bmatrix} \dfrac{\partial}{\partial a_1} \\ \dfrac{\partial}{\partial a_2} \\ \dfrac{\partial}{\partial a_3} \end{bmatrix}.$$

We shall assume that the gradient operates only on objects to its right. "Row vectors" are formed by taking the transpose of vectors:

$$a^{\mathsf{T}} = [a_1, a_2, a_3].$$

Thus the inner product of two vectors a and b is

$$a^{\mathsf{T}} b = a_i b_i.$$

Note that the order of the vectors a and b in the inner product does not matter. However, the divergence of a vector v is written

$$\nabla_a^{\mathsf{T}} v = \frac{\partial v_i}{\partial a_i}.$$

In this expression, it is crucial that v appear to the right of ∇_a.

Matrices are arrays of vectors. One very useful matrix is the identity matrix, of which the columns are the Euclidean axis vectors and the individual entries are the Kronecker deltas:

$$I = [e_1, e_2, e_3] = \begin{bmatrix} \delta_{11} & \delta_{12} & \delta_{13} \\ \delta_{21} & \delta_{22} & \delta_{23} \\ \delta_{31} & \delta_{32} & \delta_{33} \end{bmatrix}.$$

The trace of a matrix A is the sum of its diagonal entries:

$$\operatorname{tr}(A) = e_i^{\mathsf{T}} A e_i = A_{ii}.$$

Another matrix invariant is the determinant, which will be denoted by $|A|$ or by $\det A$.

The outer product of two vectors is

$$ab^{\mathsf{T}} = \begin{bmatrix} a_1 \\ a_2 \\ a_3 \end{bmatrix} [\beta_1, \beta_2, \beta_3] = \begin{bmatrix} a_1\beta_1 & a_1\beta_2 & a_1\beta_3 \\ a_2\beta_1 & a_2\beta_2 & a_2\beta_3 \\ a_3\beta_1 & a_3\beta_2 & a_3\beta_3 \end{bmatrix}.$$

In particular, the matrix of derivatives of a vector x with respect to a vector a is

$$\frac{\partial x}{\partial a} = (\nabla_a x^{\mathsf{T}})^{\mathsf{T}} = \begin{bmatrix} \dfrac{\partial x_1}{\partial a_1} & \dfrac{\partial x_1}{\partial a_2} & \dfrac{\partial x_1}{\partial a_3} \\ \dfrac{\partial x_2}{\partial a_1} & \dfrac{\partial x_2}{\partial a_2} & \dfrac{\partial x_2}{\partial a_3} \\ \dfrac{\partial x_3}{\partial a_1} & \dfrac{\partial x_3}{\partial a_2} & \dfrac{\partial x_3}{\partial a_3} \end{bmatrix}.$$

Throughout the remainder of this paper, time will be denoted by the Greek letter τ. We shall let a denote the Lagrangian coordinate, namely the location of a particle in its original Cartesian configuration. (Curvilinear coordinate systems, such as cylindrical and spherical coordinates, can be treated with the inclusion of the appropriate metric coefficients. We have omitted these terms for simplicity.) Obviously, a is independent of τ. We shall let x denote the Eulerian coordinate, namely, the current location of the particle. In Lagrangian coordinates, we consider the current position x of a particle to be a function of time τ and its original position a. The notation $d/d\tau$ denotes the material (total time) derivative, while $\partial/\partial\tau$ denotes the partial time derivative; this distinction is important only in Eulerian coordinates, where the dependent variables are taken to be functions of τ and x. We shall denote the velocity of a particle by

$$v = \frac{dx}{d\tau}.$$

In Lagrangian coordinates, the velocity is a function of a and τ, while in Eulerian coordinates it is a function of x and τ. In Lagrangian coordinates, we can also define the deformation gradient

$$F = \frac{\partial x}{\partial a}.$$

We assume that the determinant of F is positive, so that the motion has not turned the material inside-out and so that the correspondence between Lagrangian and Eulerian coordinates is invertible. The inverse of the deformation gradient can, by application of the inverse mapping theorem, be considered a function of x and τ for applications in Eulerian coordinates.

3. Conservation Laws

The motion of a solid is determined by the conservation of mass, momentum, and energy, together with the equations of state for the material. In this section of the paper, we will state the conservation laws without derivation. The interested reader can find a useful discussion of the derivation of these conservation laws, together with their expression in conservation form for Eulerian coordinates, in [11] or [12].

In the equations to follow, we shall denote the mass density by ρ, the force per unit mass acting on the body by f, the stress by S, the internal energy per unit mass by ϵ, and the radiative heat transfer per unit mass and unit time by ω. (More generally, f and ω might include diffusive terms, such as viscous forces and heat diffusion, that depend on the conserved variables.) As appropriate, we will subscript these variables by E or L to denote the relevant frame of reference.

3.1. Eulerian Forms

Conservation of mass in Eulerian coordinates can be written as the continuity equation or in conservation form:

$$0 = \frac{d\rho_E}{d\tau} + \rho_E \nabla_x^T v \quad \text{continuity equation,}$$
$$0 = \frac{\partial \rho_E}{\partial \tau} + \nabla_x^T (v\rho_E) \quad \text{conservation of mass.} \tag{3.1}$$

Conservation of momentum can be written as Newton's second law or in conservation form:

$$f^T = \frac{dv^T}{d\tau} - \frac{1}{\rho_E} \nabla_x^T S_E \quad \text{Newton's second law,}$$
$$\rho_E f^T = \frac{\partial \rho_E v^T}{\partial \tau} + \nabla_x^T (v\rho_E v^T - S_E) \quad \text{conservation of momentum.} \tag{3.2}$$

Finally, conservation of energy can be written as the first law of thermodynamics or in conservation form:

$$\omega = \frac{d\epsilon}{d\tau} - \frac{\operatorname{tr}\left(S_E \frac{\partial v}{\partial x}\right)}{\rho_E} \quad \text{first law of thermodynamics,}$$
$$\rho_E(\omega + f^T v) = \frac{\partial \rho_E(\epsilon + \frac{1}{2} v^T v)}{\partial \tau} + \nabla_x^T (v\rho_E[\epsilon + \tfrac{1}{2} v^T v] - S_E v) \quad \text{conservation of energy.} \tag{3.3}$$

3.2. Lagrangian Forms

Given a system of conservation laws written in the Eulerian frame of reference,

$$\frac{\partial u^T}{\partial \tau} + \nabla_x^T G^T = r^T,$$

we can rewrite the system in the Lagrangian frame of reference as follows:

$$\frac{\partial |F| u^T}{\partial \tau} + \nabla_a^T (|F| F^{-1}[G^T - v u^T]) = |F| r^T. \tag{3.4}$$

These results suggest that the Lagrangian density and stress should be related to the Eulerian density and stress by

$$\rho_L = \rho_E |F|,$$
$$S_L = F^{-1} S_E F^{-T} |F|. \tag{3.5}$$

(S_L is commonly called the second Piola-Kirchhoff stress, and S_E is commonly called the Cauchy stress.) Then the Lagrangian form of conservation of mass is

$$0 = \frac{d\rho_L}{d\tau} \quad \text{continuity equation,}$$
$$0 = \frac{\partial \rho_L}{\partial \tau} \quad \text{conservation of mass.}$$

The Lagrangian form of conservation of momentum is

$$f^T = \frac{dv^T}{d\tau} - \frac{1}{\rho_L} \nabla_a^T (S_L F^T) \quad \text{Newton's second law,}$$
$$\rho_L f^T = \frac{\partial \rho_L v^T}{\partial \tau} - \nabla_a^T (S_L F^T) \quad \text{conservation of momentum.} \tag{3.6}$$

The Lagrangian form of conservation of energy is

$$\omega = \frac{d\epsilon}{d\tau} - \frac{\operatorname{tr}\left(S_L F^T \frac{\partial v}{\partial a}\right)}{\rho_L} \quad \text{first law of thermodynamics,}$$
$$\rho_L(\omega + f^T v) = \frac{\partial \rho_L(\epsilon + \frac{1}{2} v^T v)}{\partial \tau} - \nabla_a^T (S_L F^T v) \quad \text{conservation of energy.} \tag{3.7}$$

4. Equations of State

There are two kinds of equations of state that are needed to help to close the system of conservation laws. The first is called a *kinetic equation of state*, and relates stress to other important variables in the motion, such as the deformation gradient. The second is the *caloric equation of state*, relating the internal energy to quantities such as temperature. Under ideal circumstances, these equations of state obey the second law of thermodynamics, which requires that the time rate of change of the entropy production is non-negative.

For lucid but dated surveys of the literature on constitutive models for elastic materials, we refer the reader to the books by Malvern (see [30]) and Fung (see [13]). We shall attempt to adopt as general an approach to the equations of state as possible without sacrificing clarity of exposition. Further, since our goal is to examine the structure of waves in solids, we shall avoid a discussion of the diffusive effects present in real materials. The inclusion of such effects in the models would tend to obscure the degree to which we are controlling the numerical diffusion in our computational schemes and would not introduce significant complications into the numerical method.

We assume that the kinetic equation can either be differentiated in time or expressed directly in the rate form

$$\frac{dS_E e_i}{d\tau} = -\tilde{\mathbf{H}}_{ij} F \frac{\partial F^{-1} e_j}{\partial \tau} + \tilde{\mathbf{h}}_i \frac{d\theta}{d\tau}. \tag{4.1}$$

Here, θ is the absolute temperature. If the derivatives of S_E with respect to F^{-1} and θ exist, then we can formally identify the matrices

$$\tilde{\mathbf{H}}_{ij} = -\frac{\partial S_E e_i}{\partial F^{-1} e_j} F^{-1}, \tag{4.2}$$

(note that $\tilde{\mathbf{H}}_{ij}$ is a matrix, not the i, j entry of a matrix), and the vectors

$$\tilde{\mathbf{h}}_i = \frac{\partial S_E e_i}{\partial \theta}. \tag{4.3}$$

The equivalent form for the kinetic equation of state in the Lagrangian frame is (1.2), where we formally identify (when the derivatives exist)

$$\mathbf{H}_{ij} = \frac{\partial F S_L e_i}{\partial F e_j} \quad , \quad \mathbf{h}_i = \frac{\partial F S_L e_i}{\partial \theta}. \tag{4.4}$$

These forms (1.2) and (4.1) are broad enough to encompass a very large class of constitutive models; in particular, it allows us to treat the models used most often in the numerical study of plasticity.

Constitutive theory makes very specific demands on the form of kinetic equations of state, demands that we are not able to display in (1.2) or (4.1). One is that the constitutive law should be frame-indifferent, so that a time-dependent orthogonal rotation of the frame of reference induces the correct similarity transformation in the stress. This requirement forms the basis of simple (elastic) materials; see [47]. Another useful notion is that there is a strain energy function, formed with respect to a homogeneous stress-free natural state, so that its time derivative is equal to the trace term in the first law of thermodynamics (3.3) or (3.7). This requirement forms the basis of hyperelastic materials; see [47]. The notion of a hyperelastic material is very useful in developing variational principles that are important in finite element analysis for static problems. Furthermore, this notion can be generalized to include thermal effects and plasticity; see [40]. Unfortunately, hyperelastic models have not been used as extensively in applied computations involving plasticity. Nevertheless, the constitutive laws for these kinds of elastic models could easily be differentiated with respect to time and expressed in the forms (1.2) or (4.1), for the purposes of developing the quasilinear forms in Section 5.

Another useful class of constitutive models is given in rate form. This class of models is most easily fit to laboratory data, where the data commonly take the form of measurement of changes in stress due to changes in strain (or vice versa) in the Eulerian frame of reference. These models rarely satisfy the second law of thermodynamics, but they are able to reproduce the laboratory data; their proponents suggest that these models are accurate even though they are thermodynamically inconsistent.

Even though the models used for plasticity may violate thermodynamics, for our purposes they may be acceptable if they satisfy two fundamental principles. One is that they must lead to hyperbolic systems, so that initial value problems are well-posed. This point is seldom addressed in engineering literature, and serves as the focal point of the discussion in Section 6 below. Our other requirement is that the models must be frame-indifferent.

There are other useful properties that stress rates should possess; see [24]. One is due to Prager, who suggested in [37] that if the stress rate is zero, then the eigenvalues of the stress should be constant. Two such stress rates are the Jaumann stress rate and the Green-Naghdi stress rate. The former is easy to compute (see [20], [22]), and its effect on the acoustic tensor, although nonsymmetric, is easy to determine (see Section 6.1 below). However, the Jaumann stress rate has no conjugate measure of finite strain (see [3]), and does not lead to a symmetric stiffness matrix; see [31]. Further, kinematic hardening causes oscillatory response in the back stress during simple shear; see [24], [34]). For this and other reasons, the Jaumann stress rate has been replaced by the Green-Naghdi stress rate in some numerical computations. However, the Green-Naghdi stress rate is significantly more expensive in three-dimensional computations, and its effect on the acoustic

tensor (also nonsymmetric) is difficult to analyze in three dimensions. Mehrabadi and Nemat-Nasser in [32] have shown how to relate the spin tensor in the Green-Naghdi stress rate to the spin tensor for the Jaumann stress rate; this formula is complicated, but proves that the required derivatives of terms in the acoustic tensor for the Green-Naghdi stress rate actually exist and can be employed in computations. Another objective stress rate is the Truesdell stress rate; see [35], [46]. This stress rate arises naturally from hyperelastic constitutive laws and leads to a symmetric acoustic tensor; however, it fails to satisfy Prager's condition of constant eigenvalues of Cauchy stress for zero stress rate. This is one reason why it is not commonly used in computations.

Our demands on the caloric equation of state are less stringent. We assume that the internal energy is a function of the absolute temperature θ and the deformation gradient F, in such a way that the partial derivatives

$$\gamma = \frac{\partial \epsilon}{\partial \theta} \quad , \quad \mathbf{c}_j^{\mathrm{T}} = \frac{\partial \epsilon}{\partial Fe_j} \tag{4.5}$$

are available. This class of caloric equations of state includes, for example, ideal thermoelastic solids.

5. Characteristic Analysis of the Equations of Motion

In this section we shall write the complete systems of equations in first-order conservation form, and determine the characteristic speeds and characteristic directions of the motion. Our purpose in this section of the paper is not to reproduce at length the classical results relating the characteristic speeds to the square roots of the eigenvalues of the acoustic tensors. We have other needs that are not met by the existing literature.

In order to apply modern numerical techniques for shock-capturing, it is necessary to write the equations of motion in *first-order conservation form*, and to find associated quaslinear forms with the correct wavespeeds for characteristic tracing. Our approach to writing the equations in first-order conservation form requires the use of the deformation gradient as a conserved quantity; however, the constraint that the deformation gradient be the gradient of a deformation introduces complications into the selection of the conservation forms and quasilinear forms of the equations of motion, as we shall see below.

For each frame of reference, we shall follow the same order of presentation. First, we shall assemble the system of conservation laws in the form appropriate for a conservative difference method. In addition to this system of conservation laws we shall write a stress-rate equation, the careful integration of which could determine the value of stress at various time levels. (Here, we are more concerned in selecting a form for the stress-rate equation that is instructive for our characteristic analysis, rather than one appropriately structured for frame-indifferent time integration.) Afterward, we shall rewrite the system of conservation laws in terms of a list of unknowns that are useful in evaluating the flux in the conservation law. The analysis of the characteristic structure of the conservation laws will be performed with respect to these "flux variables."

5.1. Lagrangian Analysis

5.1.1. Conservation Form

Our Lagrangian system of equations consists of four equations, (3.7)-(3.8), governing conservation of momentum and energy, as well as nine equations, (1.3), also in conservation form, expressing equality of mixed partial derivatives in space and time. This allows us to write a system of thirteen conservation laws

$$\frac{\partial u_{\mathrm{L}}^{\mathrm{T}}}{\partial \tau} + \nabla_a^{\mathrm{T}} G_{\mathrm{L}}^{\mathrm{T}} = r_{\mathrm{L}}^{\mathrm{T}}, \tag{5.1}$$

where

$$u_{\mathrm{L}} = \begin{bmatrix} \mathrm{v}\rho_{\mathrm{L}} \\ (\epsilon + \frac{1}{2}\mathrm{v}^{\mathrm{T}}\mathrm{v})\rho_{\mathrm{L}} \\ Fe_1 \\ Fe_2 \\ Fe_3 \end{bmatrix}, \quad G_{\mathrm{L}} = \begin{bmatrix} -FS_{\mathrm{L}} \\ -\mathrm{v}^{\mathrm{T}}FS_{\mathrm{L}} \\ -\mathrm{v}e_1^{\mathrm{T}} \\ -\mathrm{v}e_2^{\mathrm{T}} \\ -\mathrm{v}e_3^{\mathrm{T}} \end{bmatrix}, \quad r_{\mathrm{L}} = \begin{bmatrix} f\rho_{\mathrm{L}} \\ (\omega + f^{\mathrm{T}}\mathrm{v})\rho_{\mathrm{L}} \\ 0 \\ 0 \\ 0 \end{bmatrix}. \tag{5.2}$$

In addition to this system of conservation laws, we also have the ordinary differential equations (1.2) for the stress. These ordinary differential equations can be considered to be a prescription for evaluating the stress and its derivatives; indeed, if the stress were described by a hyperelastic model, there would be no need to integrate (1.2) in the course of solving the equations of motion. (See [40] for a discussion of the advantages of an approach of this form in the context of plasticity.) At any rate, the ordinary differential equations (1.2) do not contribute to issues concerning the classification of the system of conservation laws. Finally, we note that the curl condition (1.4) is assumed to hold; this is an initial-value condition that may need to be enforced occasionally during the time-stepping procedure of a numerical method.

Note that all of the entries of u_{L} and G_{L} can be considered to be functions of

$$w_{\mathrm{L}} = \begin{bmatrix} \mathrm{v} \\ \theta \\ Fe_1 \\ Fe_2 \\ Fe_3 \end{bmatrix}.$$

Thus the system of conservation laws (5.1) is hyperbolic if and only if the matrix

$$\frac{\partial G_L n_L}{\partial u_L} = \frac{\partial G_L n_L}{\partial w_L}\left(\frac{\partial u_L}{\partial w_L}\right)^{-1}$$

has real eigenvalues for any unit vector n_L. Equations (5.1) and (5.2) pose the proper form for purposes of conserving the appropriate quantities in our numerical algorithm, and for purposes of bequeathing the correct shock speeds to the computational results. However, another step of the second-order Godunov method requires the computation of monotonized slopes in characteristic quantities for the purposes of constructing left and right states in a Riemann problem. (See Section 7 below.) We want the results of the characteristic tracing step to provide the information needed to construct physically meaningful fluxes at the cell interfaces. For this step of the computation, it is useful to write the equations of motion in non-conservation form. This form of the equations obtains the same characteristic speeds as in (5.1) and (5.2), but the characteristic directions we shall determine below are far more simple.

5.1.2. Quasilinear Form

We can use the equality of mixed partials (1.3) to write the system of equations (5.1) and (5.2) in the form

$$\begin{bmatrix} I\rho_L & 0 & 0 & 0 & 0 \\ 0 & \rho_L\gamma & 0 & 0 & 0 \\ 0 & -\mathbf{h}_1 & I & 0 & 0 \\ 0 & -\mathbf{h}_2 & 0 & I & 0 \\ 0 & -\mathbf{h}_3 & 0 & 0 & I \end{bmatrix} \frac{\partial}{\partial \tau} \begin{bmatrix} \mathbf{v} \\ \theta \\ FS_L e_1 \\ FS_L e_2 \\ FS_L e_3 \end{bmatrix}$$

$$+ \begin{bmatrix} 0 & 0 & -I\delta_{1j} & -I\delta_{2j} & -I\delta_{3j} \\ -\rho_L\gamma\mathbf{b}_j^T & 0 & 0 & 0 & 0 \\ -\mathbf{H}_{1j} & 0 & 0 & 0 & 0 \\ -\mathbf{H}_{2j} & 0 & 0 & 0 & 0 \\ -\mathbf{H}_{3j} & 0 & 0 & 0 & 0 \end{bmatrix} \frac{\partial}{\partial a_j} \begin{bmatrix} \mathbf{v} \\ \theta \\ FS_L e_1 \\ FS_L e_2 \\ FS_L e_3 \end{bmatrix} = \begin{bmatrix} f\rho_L \\ \omega\rho_L \\ 0 \\ 0 \\ 0 \end{bmatrix}, \tag{5.3}$$

where γ and $\mathbf{c}_j$ are defined by (4.5), and

$$\mathbf{b}_j^T = \frac{1}{\gamma\rho_L}(e_j^T S_L F^T - \rho_L \mathbf{c}_j^T). \tag{5.4}$$

Also recall that when the derivatives exist, we can formally identify $\mathbf{H}_{ij}$ and $\mathbf{h}_i$ as in (4.4). In order to analyze the hyperbolicity of this system, we assume (without loss of generality) that the coordinate system has been rotated so that the normal n_L is aligned with the first coordinate axis. Then hyperbolicity requires

$$B = \begin{bmatrix} I\rho_L & 0 & 0 & 0 & 0 \\ 0 & \rho_L\gamma & 0 & 0 & 0 \\ 0 & -\mathbf{h}_1 & I & 0 & 0 \\ 0 & -\mathbf{h}_2 & 0 & I & 0 \\ 0 & -\mathbf{h}_3 & 0 & 0 & I \end{bmatrix}^{-1} \begin{bmatrix} 0 & 0 & -I & 0 & 0 \\ -\rho_L\gamma\mathbf{b}_1^T & 0 & 0 & 0 & 0 \\ -\mathbf{H}_{11} & 0 & 0 & 0 & 0 \\ -\mathbf{H}_{21} & 0 & 0 & 0 & 0 \\ -\mathbf{H}_{31} & 0 & 0 & 0 & 0 \end{bmatrix}$$

$$= \begin{bmatrix} 0 & 0 & -I\frac{1}{\rho_L} & 0 & 0 \\ -\mathbf{b}_1^T & 0 & 0 & 0 & 0 \\ -\mathbf{A}_{11} & 0 & 0 & 0 & 0 \\ -\mathbf{A}_{21} & 0 & 0 & 0 & 0 \\ -\mathbf{A}_{31} & 0 & 0 & 0 & 0 \end{bmatrix}$$

to have real eigenvalues. Here we have used the notation

$$\mathbf{A}_{ij} = \mathbf{H}_{ij} + \mathbf{h}_i\mathbf{b}_j^T. \tag{5.5}$$

It is obvious that seven of the eigenvalues of B are zero, with right eigenvectors corresponding to the appropriate columns of the identity matrix. This deflation process can be continued, reducing the problem to finding the eigenvectors and eigenvalues of $\mathbf{A}_{11}$:

$$\mathbf{A}_{11}X = X\Lambda^2\rho_L. \tag{5.6}$$

Afterward, we can assemble the eigenvectors of B:

$$\begin{bmatrix} 0 & 0 & -I\frac{1}{\rho_L} & 0 & 0 \\ -\mathbf{b}_1^T & 0 & 0 & 0 & 0 \\ -\mathbf{A}_{11} & 0 & 0 & 0 & 0 \\ -\mathbf{A}_{21} & 0 & 0 & 0 & 0 \\ -\mathbf{A}_{31} & 0 & 0 & 0 & 0 \end{bmatrix} \begin{bmatrix} X\Lambda & 0 & -X\Lambda & 0 & 0 \\ \mathbf{b}_1^T X & 1 & \mathbf{b}_1^T X & 0 & 0 \\ X\Lambda^2\rho_L & 0 & X\Lambda^2\rho_L & 0 & 0 \\ \mathbf{A}_{21}X & 0 & \mathbf{A}_{21}X & I & 0 \\ \mathbf{A}_{31}X & 0 & \mathbf{A}_{31}X & 0 & I \end{bmatrix}$$

$$= \begin{bmatrix} X\Lambda & 0 & -X\Lambda & 0 & 0 \\ \mathbf{b}_1^T X & 1 & \mathbf{b}_1^T X & 0 & 0 \\ X\Lambda^2\rho_L & 0 & X\Lambda^2\rho_L & 0 & 0 \\ \mathbf{A}_{21}X & 0 & \mathbf{A}_{21}X & I & 0 \\ \mathbf{A}_{31}X & 0 & \mathbf{A}_{31}X & 0 & I \end{bmatrix} \begin{bmatrix} -\Lambda & 0 & 0 & 0 & 0 \\ 0 & 0 & 0 & 0 & 0 \\ 0 & 0 & \Lambda & 0 & 0 \\ 0 & 0 & 0 & 0 & 0 \\ 0 & 0 & 0 & 0 & 0 \end{bmatrix}. \tag{5.7}$$

In summary, if the system is hyperbolic, then there are seven characteristic speeds equal to zero, and six other characteristic speeds occurring in plus/minus pairs. An eigenvector deficiency occurs if any of the speeds in the plus/minus pairs is equal to zero.

From this analysis, we can determine the circumstances under which the system (5.3) is hyperbolic. In order to do so, we shall use the definitions (5.4) and (5.5), as well as an orthogonal change of coordinates, to rewrite equation (5.6) in the form

$$A_L X = \left[\mathbf{H}_i n_i n_i \frac{1}{\rho_L} + h_i \frac{1}{\rho_L} n_i b_i^T \right] X = X \Lambda_L^2, \quad \text{(summed over } i\text{)} \tag{5.8}$$

where n_i are the entries of an arbitrary unit vector. The equations of motion are hyperbolic if and only if equation (5.8) holds with a real matrix Λ_L for any unit vector n_L. If we can assume that the derivatives of the first Piola-Kirchhoff stress FS_L exist with respect to F and θ, then we can rewrite this result in the form

$$A_L X = \left[\frac{\partial F S_L n_L}{\partial F n_L} \frac{1}{\rho_L} + \frac{\partial F S_L n_L}{\partial \theta} \frac{1}{\gamma \rho_L^2} \left(n_L^T S_L F^T - \rho_L \frac{\partial \epsilon}{\partial F n_L} \right) \right] X = X \Lambda_L^2. \tag{5.8*}$$

This condition for positive eigenvalues is consistent with Truesdell's notion of a strongly elliptic function for isothermal isotropic elastic solids (see [47]), and must be verified for the individual constitutive model and caloric equations of state. In the discussion to follow, we will call A_L the *Lagrangian acoustic tensor*, even though the conventional acoustic tensor in the continuum mechanics literature ignores thermal effects.

Before concluding the Lagrangian characteristic analysis, we note that in some applications (such as gas dynamics) the stress is formulated directly in terms of the internal energy. In other applications, the caloric equation of state may be difficult to solve for temperature. Thus, there are cases in which it may be advantageous to perform a characteristic analysis using ϵ instead of θ. The form of the characteristic analysis in such a case can be related to the analysis above by taking $\gamma = 1$ and $c_j = 0$; that is, no separate characteristic analysis is needed.

5.2. Eulerian Analysis

Next, we turn to the problem of identifying the characteristic speeds for the Eulerian formulation of the system of conservation laws. Here, we need to make sure that we have all of the variables needed to evaluate the flux in our quasilinear equations. We shall also need to be careful about the correct form of the equality of mixed partial derivatives, in order for the Eulerian characteristic speeds to be properly related to the Lagrangian speeds.

5.2.1. Conservation Form

The Eulerian form of the conservation equations is

$$\frac{\partial u_E^T}{\partial \tau} + \nabla_x^T G_E^T = r_E^T, \tag{5.9}$$

where

$$u_E = \begin{bmatrix} \rho_E \\ v\rho_E \\ (\epsilon + \frac{1}{2} v^T v)\rho_E \\ F^{-1} e_1 \\ F^{-1} e_2 \\ F^{-1} e_3 \end{bmatrix}, \quad G_E = \begin{bmatrix} \rho_E v^T \\ v\rho_E v^T - S_E \\ (\epsilon + \frac{1}{2} v^T v)\rho_E v^T - v^T S_E \\ F^{-1} v e_1^T \\ F^{-1} v e_2^T \\ F^{-1} v e_3^T \end{bmatrix}, \tag{5.10}$$

$$r_E = \begin{bmatrix} 0 \\ f\rho_E \\ (\omega + f^T v)\rho_E \\ 0 \\ 0 \\ 0 \end{bmatrix}.$$

The last nine equations in this system come from the equality of mixed partial derivatives (1.5), which has been chosen from several alternatives in order to minimize the number of variables needed in the quasilinear form (5.11) below. In addition to this system of equations, we have the stress-rate equation (4.1).

Note that there is a difficulty with this formulation of the conservation laws in the Eulerian frame of reference. The stress-rate equation (4.1) uses the equality of mixed partials in the form (1.7), while the system of conservation laws (5.9) and (5.10) uses the form (1.5). Further, a direct characteristic analysis of (5.9) and (5.10) produces some characteristic speeds that are not the proper analogues of the Lagrangian speeds. It would have been tempting to apply the equation (3.4) for change of frame of reference to the Lagrangian equation (1.3) for equality of mixed partial derivatives, and derive

$$\frac{\partial |F^{-1}| e_i |F^T}{\partial \tau} + \nabla_x^T (v |F^{-1}| e_i^T F^T - F e_i |F^{-1}| v^T) = 0$$

for the Eulerian form of equality of mixed partial derivatives. This is the form of equality of mixed partial derivatives chosen by Plohr and Sharp in [36]. However,

direct characteristic analysis of this conservation law, by itself, does not obtain the proper characteristic speeds, either.

In both the Lagrangian and Eulerian frames of reference, the system of conservation laws must be augmented by equations representing equality of mixed second-order partial derivatives in space. The obvious purpose of these constraints in the Lagrangian frame is to guarantee that the deformation gradient is the gradient of a vector field, namely the current particle position. In the Eulerian frame, the inverse deformation gradient is likewise constrained. The need to impose these constraints has been observed by several authors, such as Hanyga in [17], and Plohr and Sharp in [36]. With these constraints, the equations of motion in first-order form are fully and correctly specified. However, the above authors do not consider the issue of how to impose these constraints properly in a characteristic analysis.

Since we are interested in using characteristic information in the development of a second-order Godunov method, we shall determine the characteristic speeds very carefully. In order to write the equations of motion in conservation form, we might prefer equation (1.5) for the evolution of the inverse deformation gradient, while for purposes of the characteristic analysis we shall find that (1.7) is better. The curl condition (1.6) can be used to show that (1.7) and (1.5) are equivalent. In this regard, we note that if the curl of the inverse deformation gradient is zero in the initial data, then it is zero for all time. (The proof of this fact uses the fact that the curl of the velocity gradient is zero.) Numerically, it may be necessary to enforce this curl condition occasionally during the computation, much as the div B condition in magnetohydrodynamics is handled. (In fact, experience with numerical methods for magnetohydrodynamics indicates that catastrophic failure of the integration can occur if div $B = 0$ is not enforced during the timestepping procedure.) Another option is to replace the appropriate equations in (5.9) and (5.10) with the equations (1.7), which are not in conservation form; this necessitates some modification to the conservative difference step in the Godunov scheme. The proper form of the Eulerian equations of motion for numerical purposes will be the subject of a future paper.

5.2.2. Quasilinear Form

Looking at (5.10), we see that the flux depends on the variables

$$w_E = \begin{bmatrix} \rho_E \\ \mathbf{v} \\ \theta \\ S_E e_1 \\ S_E e_2 \\ S_E e_3 \\ F^{-1}\mathbf{v} \end{bmatrix}.$$

Thus the Eulerian frame requires more variables to evaluate the flux than does the

Lagrangian frame, and even more variables than are conserved in (5.9) and (5.10). We can write the system for these flux variables in matrix-vector form as follows:

$$\begin{bmatrix} 1 & 0 & 0 & 0 & 0 & 0 & 0 \\ 0 & I\rho_E & 0 & 0 & 0 & 0 & 0 \\ 0 & 0 & \rho_E\gamma & 0 & 0 & 0 & 0 \\ 0 & 0 & -\tilde{\mathbf{h}}_1 & I & 0 & 0 & 0 \\ 0 & 0 & -\tilde{\mathbf{h}}_2 & 0 & I & 0 & 0 \\ 0 & 0 & -\tilde{\mathbf{h}}_3 & 0 & 0 & I & 0 \\ 0 & -F^{-1} & 0 & 0 & 0 & 0 & I \end{bmatrix} \frac{\partial}{\partial \tau} \begin{bmatrix} \rho_E \\ \mathbf{v} \\ \theta \\ S_E e_1 \\ S_E e_2 \\ S_E e_3 \\ F^{-1}\mathbf{v} \end{bmatrix}$$

$$+ \begin{bmatrix} \mathbf{v}_j & \rho_E e_j^T & 0 & 0 & 0 & 0 & 0 \\ 0 & I\rho_E \mathbf{v}_j & 0 & -I\delta_{1j} & -I\delta_{2j} & -I\delta_{3j} & 0 \\ 0 & \gamma\rho_E \tilde{\mathbf{b}}_j^T & \gamma\rho_E \mathbf{v}_j & 0 & 0 & 0 & 0 \\ 0 & -\tilde{\mathbf{H}}_{1j} & -\tilde{\mathbf{h}}_1 \mathbf{v}_j & I\mathbf{v}_j & 0 & 0 & 0 \\ 0 & -\tilde{\mathbf{H}}_{2j} & -\tilde{\mathbf{h}}_2 \mathbf{v}_j & 0 & I\mathbf{v}_j & 0 & 0 \\ 0 & -\tilde{\mathbf{H}}_{3j} & -\tilde{\mathbf{h}}_3 \mathbf{v}_j & 0 & 0 & I\mathbf{v}_j & 0 \\ 0 & 0 & 0 & 0 & 0 & 0 & I\mathbf{v}_j \end{bmatrix} \frac{\partial}{\partial x_j} \begin{bmatrix} \rho_E \\ \mathbf{v} \\ \theta \\ S_E e_1 \\ S_E e_2 \\ S_E e_3 \\ F^{-1}\mathbf{v} \end{bmatrix} \tag{5.11}$$

$$= \begin{bmatrix} 0 \\ f\rho_E \\ \omega\rho_E \\ 0 \\ 0 \\ 0 \\ 0 \end{bmatrix},$$

where

$$\tilde{\mathbf{b}}_j^T = -\frac{1}{\rho_E \gamma} \left(e_j^T S_E + \rho_E \frac{\partial \epsilon}{\partial F^{-1} e_j} F^{-1} \right),$$

and $\tilde{\mathbf{H}}_{ij}$ and $\tilde{\mathbf{h}}_i$ are given in (4.1). Recall that when the derivatives exist, we can formally identify $\tilde{\mathbf{H}}_{ij}$ and $\tilde{\mathbf{h}}_i$ as in (4.2) and (4.3). In order for the system (5.11) to be hyperbolic, we require

$$\tilde{B} = \begin{bmatrix} \mathbf{v}_1 & \rho_E e_1^T & 0 & 0 & 0 & 0 & 0 \\ 0 & I\mathbf{v}_1 & 0 & -I\frac{1}{\rho_E} & 0 & 0 & 0 \\ 0 & \tilde{\mathbf{b}}_1^T & \mathbf{v}_1 & 0 & 0 & 0 & 0 \\ 0 & -\tilde{\mathbf{A}}_{11} & 0 & I\mathbf{v}_1 & 0 & 0 & 0 \\ 0 & -\tilde{\mathbf{A}}_{21} & 0 & 0 & I\mathbf{v}_1 & 0 & 0 \\ 0 & -\tilde{\mathbf{A}}_{31} & 0 & 0 & 0 & I\mathbf{v}_1 & 0 \\ 0 & F^{-1}\mathbf{v}_1 & 0 & -F^{-1}\frac{1}{\rho_E} & 0 & 0 & I\mathbf{v}_1 \end{bmatrix}$$

to real eigenvalues. Here, we have defined

$$\tilde{\mathbf{A}}_{ij} = \tilde{\mathbf{H}}_{ij} - \tilde{\mathbf{h}}_i \tilde{\mathbf{b}}_j^{\mathrm{T}}.$$

By shifting the eigenvalues and deflating, we derive the interesting eigenvalues from

$$\tilde{\mathbf{A}}_{11} X = X \Lambda^2 \rho_{\mathrm{E}}. \tag{5.12}$$

Assuming that we can solve (5.12) with real nonsingular Λ, we can solve the eigenproblem for $\tilde{B}$:

$$\tilde{B} \begin{bmatrix} 1 & -\rho_{\mathrm{E}} e_1^{\mathrm{T}} X & 0 & -\rho_{\mathrm{E}} e_1^{\mathrm{T}} X & 0 & 0 & 0 \\ 0 & X\Lambda & 0 & -X\Lambda & 0 & 0 & 0 \\ 0 & -\tilde{\mathbf{b}}_1^{\mathrm{T}} X & 1 & -\tilde{\mathbf{b}}_1^{\mathrm{T}} X & 0 & 0 & 0 \\ 0 & X\Lambda^2 \rho_{\mathrm{E}} & 0 & X\Lambda^2 \rho_{\mathrm{E}} & 0 & 0 & 0 \\ 0 & \tilde{\mathbf{A}}_{21} X & 0 & \tilde{\mathbf{A}}_{21} X & I & 0 & 0 \\ 0 & \tilde{\mathbf{A}}_{31} X & 0 & \tilde{\mathbf{A}}_{31} X & 0 & I & 0 \\ 0 & -F^{-1} X (I\mathrm{v}_1 - \Lambda) & 0 & -F^{-1} X (I\mathrm{v}_1 + \Lambda) & 0 & 0 & I \end{bmatrix}$$

$$= \begin{bmatrix} 1 & -\rho_{\mathrm{E}} e_1^{\mathrm{T}} X & 0 & -\rho_{\mathrm{E}} e_1^{\mathrm{T}} X & 0 & 0 & 0 \\ 0 & X\Lambda & 0 & -X\Lambda & 0 & 0 & 0 \\ 0 & -\tilde{\mathbf{b}}_1^{\mathrm{T}} X & 1 & -\tilde{\mathbf{b}}_1^{\mathrm{T}} X & 0 & 0 & 0 \\ 0 & X\Lambda^2 \rho_{\mathrm{E}} & 0 & X\Lambda^2 \rho_{\mathrm{E}} & 0 & 0 & 0 \\ 0 & \tilde{\mathbf{A}}_{21} X & 0 & \tilde{\mathbf{A}}_{21} X & I & 0 & 0 \\ 0 & \tilde{\mathbf{A}}_{31} X & 0 & \tilde{\mathbf{A}}_{31} X & 0 & I & 0 \\ 0 & -F^{-1} X (I\mathrm{v}_1 - \Lambda) & 0 & -F^{-1} X (I\mathrm{v}_1 + \Lambda) & 0 & 0 & I \end{bmatrix}$$

$$\times \begin{bmatrix} \mathrm{v}_1 & 0 & 0 & 0 & 0 & 0 & 0 \\ 0 & I\mathrm{v}_1 - \Lambda & 0 & 0 & 0 & 0 & 0 \\ 0 & 0 & \mathrm{v}_1 & 0 & 0 & 0 & 0 \\ 0 & 0 & 0 & I\mathrm{v}_1 + \Lambda & 0 & 0 & 0 \\ 0 & 0 & 0 & 0 & I\mathrm{v}_1 & 0 & 0 \\ 0 & 0 & 0 & 0 & 0 & I\mathrm{v}_1 & 0 \\ 0 & 0 & 0 & 0 & 0 & 0 & I\mathrm{v}_1 \end{bmatrix}.$$

We want to find a condition that is satisfied if and only if (5.11) is hyperbolic. By a rotation of the axes, we can rewrite equation (5.12) in the form

$$A_{\mathrm{E}} X = \left[\tilde{\mathbf{H}}_{ij} n_i n_i \frac{1}{\rho_{\mathrm{E}}} + \tilde{\mathbf{h}}_i n_i \frac{1}{\rho_{\mathrm{E}}} \tilde{\mathbf{b}}_i^{\mathrm{T}} \right] X = X \Lambda_{\mathrm{E}}^2, \quad \text{(summed over } i\text{)} \tag{5.13}$$

where n_i are the entries of an arbitrary unit vector. The system (5.11) is hyperbolic if and only if for any unit vector n_{E} (5.13) is satisfied with real Λ_{E}. The characteristic speeds are either $\mathrm{v}^{\mathrm{T}} n_{\mathrm{E}}$ or $\pm \Lambda_{\mathrm{E}} + \mathrm{v}^{\mathrm{T}} n_{\mathrm{E}}$. We shall call A_{E} the *Eulerian acoustic tensor*.

If the derivatives of the Eulerian stress S_{E} exist with respect to F^{-1} and θ, then we can use (4.2) and (4.3) to rewrite (5.13) in the form

$$A_{\mathrm{E}} X = -\left[\frac{\partial S_{\mathrm{E}} n_{\mathrm{E}}}{\partial F^{-1} n_{\mathrm{E}}} F^{-1} \frac{1}{\rho_{\mathrm{E}}} - \frac{\partial S_{\mathrm{E}} n_{\mathrm{E}}}{\partial \theta} \frac{1}{\gamma \rho_{\mathrm{E}}^2} \left(n_{\mathrm{E}}^{\mathrm{T}} S_{\mathrm{E}} + \rho_{\mathrm{E}} \frac{\partial \epsilon}{\partial F^{-1} n_{\mathrm{E}}} F^{-1} \right) \right] X = X \Lambda_{\mathrm{E}}^2, \tag{5.13*}$$

5.3. Equivalence of the Lagrangian and Eulerian Formulations

From the analyses of the preceding two sections, we have seen that the Lagrangian equations are hyperbolic if and only if for any unit vector n_{L}, the Lagrangian acoustic tensor has non-negative real eigenvalues. We also have seen that the Eulerian equations are hyperbolic if and only if for any unit vector n_{E}, the Eulerian acoustic tensor has non-negative real eigenvalues. If the derivatives of stress with respect to deformation gradient and absolute temperature exist, then we can relate the Eulerian and Lagrangian acoustic tensors quite easily. Since the Lagrangian and Eulerian unit normals are related by

$$n_{\mathrm{L}} \nu = F^{\mathrm{T}} n_{\mathrm{E}}$$

for some scalar ν (see, for example, [27] or [1]), we can use the relationship (3.5) between the stress and density in the two frames of reference, the formula

$$\frac{\partial F^{-1}}{\partial \tau} = -F^{-1} \frac{\partial F}{\partial \tau} F^{-1},$$

for the derivative of an inverse, and the equation

$$\frac{\partial A^{-\mathrm{T}} n |A|}{\partial A n} = 0$$

for the derivative of the matrix of co-factors, to show that

$$A_{\mathrm{L}} \nu^2 = A_{\mathrm{E}}.$$

(Here, we have assumed that all the required derivatives of Lagrangian and Eulerian stress actually exist.) Since the matrices A_{L} and A_{E} are scalar multiples of each other, they share the same eigenvectors:

$$A_{\mathrm{L}} X = X \Lambda_{\mathrm{L}}^2 \quad , \quad A_{\mathrm{E}} X = X \Lambda_{\mathrm{E}}^2.$$

Thus we obtain the following relationship between the Lagrangian speeds and the Eulerian speeds minus the normal velocity:

$$\Lambda_{\mathrm{L}} = \Lambda_{\mathrm{E}} \| F^{\mathrm{T}} n_{\mathrm{E}} \| \quad \text{or} \quad \Lambda_{\mathrm{E}} = \Lambda_{\mathrm{L}} \frac{1}{\| F^{-\mathrm{T}} n_{\mathrm{L}} \|}.$$

6. Characteristic Analyses of Specific Material Models

In Sections 5.1 and 5.2 we reduced the characteristic analysis of the equations of motion to an eigenproblem for a 3×3 matrix. In the sections below we shall examine this eigenproblem for a few models of common usage, in order to determine whether these models lead to hyperbolic systems of equations. This discussion is not intended to be exhaustive of models for solids; instead, we are primarily concerned with determining that some of the common models for plasticity lead to hyperbolic systems. We have chosen models that are used to describe elastic-plastic solids in practice (such as in the well-known finite element codes DYNA2D and DYNA3D), in spite of the fact that these models may not obey thermodynamic conditions such as the second law. For further discussion of the use of these models in practice see [22]. We also note that the analysis in these sections is similar to that by Mandel [31], who analyzed the effect of plasticity on the characteristic speeds, but ignored the effect of the stress rates.

6.1. Elastic Laws in Rate Form

We shall use the Jaumann stress rate

$$\dot{S}_E = \frac{dS_E}{d\tau} + W^T S_E + S_E W, \tag{6.1}$$

where W is the spin tensor

$$W = \frac{1}{2}\left[\frac{\partial v}{\partial x} - \left(\frac{\partial v}{\partial x}\right)^T\right]. \tag{6.2}$$

Since W is antisymmetric, we can use it to generate an orthogonal matrix $\Omega(\tau)$, defined by the initial value problem

$$\frac{d\Omega}{d\tau} = W\Omega \quad , \quad \Omega^T\Omega|_{\tau=0} = I. \tag{6.3}$$

As a result, the Jaumann stress rate can be written in the form

$$\dot{S}_E = \Omega \frac{d\Omega^T S_E \Omega}{d\tau} \Omega^T. \tag{6.4}$$

This relation shows that the Jaumann stress is determined by rotating the rate of the unrotated stress,

$$S = \Omega S_E \Omega. \tag{6.5}$$

From (6.4), we can also see that if the Jaumann stress rate is zero, then the eigenvalues of S_E are constant.

For elastic behavior, we assume that the Jaumann stress rate is related to the rate of deformation, defined by

$$D = \frac{1}{2}\left[\frac{\partial v}{\partial x} + \left(\frac{\partial v}{\partial x}\right)^T\right], \tag{6.6}$$

through Hooke's law in rate form:

$$\dot{S}_E = D2\mu + I\left(\kappa - \frac{2\mu}{3}\right)\mathrm{tr}\, D. \tag{6.7}$$

Here, κ is the bulk modulus and μ is the shear modulus, neither of which is necessarily constant. In order to determine whether (5.9)-(5.10) is hyperbolic, we use (6.2)-(6.4) to rewrite (6.7) in the form:

$$\frac{dS_E}{d\tau} = \left[\frac{\partial v}{\partial x} + \left(\frac{\partial v}{\partial x}\right)^T\right]\mu + I\left(\kappa - \frac{2\mu}{3}\right)\mathrm{tr}\frac{\partial v}{\partial x} + \left[\frac{\partial v}{\partial x} - \left(\frac{\partial v}{\partial x}\right)^T\right]\frac{1}{2} S_E - S_E\left[\frac{\partial v}{\partial x} - \left(\frac{\partial v}{\partial x}\right)^T\right]\frac{1}{2}.$$

By a straightforward calculation, we see from this equation and (5.13) that the hyperbolicity of the equations of motion is determined by the eigenvalues of the Eulerian acoustic tensor

$$A_E = H + C,$$

where

$$H = I\frac{\mu}{\rho_E} + n_E \frac{\kappa + \frac{\mu}{3}}{\rho_E} n_E^T, \tag{6.8}$$

$$C = [In_E^T S_E n_E + S_E n_E n_E^T - n_E n_E^T S_E - S_E]\,1/2\rho_E. \tag{6.9}$$

The acoustic tensor is the sum of a symmetric matrix H that is derived from the strain rate terms, and a nonsymmetric matrix C that comes from the stress rate terms. Even though the acoustic tensor is not symmetric, we can perform a careful analysis to show that it has real positive eigenvalues.

We note that n_E is an eigenvector of the acoustic tensor, with eigenvalue $(\kappa + (4\mu/3))1/\rho_E$. We shall use deflation to determine the remaining eigenvalues. Let Q be an orthogonal matrix, the first column of which is n_E:

$$Q = [n_E, Q_2]. \tag{6.10}$$

As a result, A_E is similar to

$$Q^T A_E Q = \begin{bmatrix} \kappa + \frac{4\mu}{3} & -n_E^T S_E Q_2 \\ 0 & I(\mu + n_E^T S_E n_E \tfrac{1}{2}) - Q_2^T S_E Q_2 \tfrac{1}{2} \end{bmatrix} \frac{1}{\rho_E}.$$

The remaining eigenvalues of the acoustic tensor are eigenvalues of the 2×2 symmetric matrix

$$I \frac{\mu + n_E^T S_E n_E \tfrac{1}{2}}{\rho_E} - Q_2^T S_E Q_2 \frac{1}{2\rho_E},$$

and are therefore real; however, the equations of motion are hyperbolic if and only if these eigenvalues are non-negative. The Rayleigh quotient for this matrix takes the form

$$(\mu + n_E^T S_E n_E - z^T Q_2^T S_E Q_2 z) \frac{1}{2\rho_E},$$

where z is an arbitrary unit vector. Note that both $n_E^T S_E n_E$ and $z^T Q_2^T S_E Q_2 z$ lie between the smallest and largest eigenvalues of S_E. As a result, the remaining eigenvalues of the acoustic tensor lie between $(\mu - \sigma)/\rho_E$ and $(\mu + \sigma)/\rho_L$, where σ is the difference between the largest and smallest eigenvalues of S_E. If $\sigma < \mu$, then the acoustic tensor will have real, positive eigenvalues, and the equations of motion will be hyperbolic. Furthermore, if $\sigma < \kappa + \frac{1}{3}\mu$, then the acoustic tensor has a full set of eigenvectors. We note in Section 6.2.6 below that σ typically lies well below the value of μ.

This model can be rewritten in the Lagrangian frame of reference without any significant effort. Because of our discussion in Section 5.3 above, we can write

$$A_L = I \frac{\mu}{\rho_L} |F| \|F^{-T} n_L\|^2 + F^{-T} n_L |F| \frac{\kappa + \frac{\mu}{3}}{\rho_L} n_L^T F^{-1}$$

$$+ [I n_L^T S_L n_L + F S_L n_L N_L^T F^{-1} - F^{-T} n_L n_L^T S_L F^T - F S_L F^T \|F^{-T} n_L\|^2] \frac{1}{2\rho_L}.$$

Furthermore, it is straightforward to write the constitutive law in a form involving Lagrangian variables.

6.2. Plasticity with Isotropic Work-Hardening

6.2.1. Background on Plasticity

When materials are subjected to sufficient applied forces, the individual particles, grains, or chemical bonds in the material can be dislocated. If the applied forces are subsequently removed, the material will relax to a permanently deformed configuration. This permanent deformation is also called *plastic* deformation. The behavior of the material then becomes a function of the history of its applied loads; this phenomenon is called *hysteresis*. We shall discuss some elementary models for elastic-plastic materials. Our discussion will not incorporate the very interesting work on plasticity models for finite elastic and plastic deformations; see [16], [26], [28], [40]. We shall also ignore temperature effects in this discussion, even though it is commonly known that the work done on the material in order to cause plastic deformations contributes to an increase in the temperature of the material. (For discussion of a model with temperature effects in hyperelastic plasticity see [16].) Furthermore, we shall ignore dependence of the stress on the rate of deformation, since this will contribute to a diffusive term in the system of differential equations describing the motion. Finally, we assume that the material is isotropic, even though finite plastic deformation will usually introduce anisotropies in the material response; see [16]. These are often modeled with kinematic work-hardening, through a back-stress; we have not included these terms in our discussion below in order to simplify the exposition.

6.2.2. Elastic-Plastic Model

Our analysis in this section is based upon the general discussions of plasticity with work-hardening in [13] and [30]. Note that specific application of our numerical method to the cap model for plasticity in soils and rocks appears in [44]; the cap model involves four yield surfaces, two of which depend on the hardening parameter.

We assume initially that there is a yield function ϕ depending on the Jaumann unrotated stress (6.5) and on a work-hardening parameter χ. The purpose of the yield function is to place a constraint on the admissible values of stress for a given level of hardening. Specifically, for $\phi < 0$ the material response is assumed to be elastic. The material response is also elastic if $\phi = 0$ and the rate of deformation leads to a nonpositive rate of change of ϕ. Otherwise, the material response is plastic. For simplicity, we shall assume that the elastic rate of deformation is infinitesimal, so that the rate of deformation is the sum of the elastic and plastic rates of deformation:

$$D = D^e + D^p.$$

(The correct generalization of this equation to finite elastic and plastic deformations is described in [16].) We also assume that the elastic stress-strain relationship is given by the analogue of (6.7):

$$\dot{S}_E = D^e 2\mu + I\left(\kappa - \frac{2\mu}{3}\right)\operatorname{tr} D^e.$$

Our next goals are to describe the circumstances under which plastic loading occurs on the yield surface, and to determine the plastic rates of deformation.

During elastic response, no additional permanent deformations are introduced. Thus,

$$D^p = 0 \quad \text{and} \quad \frac{d\chi}{d\tau} = 0 \quad \text{during elastic response.}$$

Elastic response occurs in two ways: if the unrotated stress lies inside the yield surface, or if the stress lies on the yield surface and the rate of change of the yield function is non-positive. Let us give a mathematical representation of the latter condition. If the stress lies on the yield surface, meaning that $\phi(S, \chi) = 0$, then unloading (or neutral loading) occurs, and the material response is elastic, if

$$0 \geq \frac{d\phi}{d\tau} = \operatorname{tr}\left(\Phi_S \frac{dS}{d\tau}\right) + \frac{\partial\phi}{\partial\chi}\frac{d\chi}{d\tau}$$

$$= \operatorname{tr}\left(\Phi_S\left[\Omega^T D\Omega 2\mu + I\left(\kappa - \frac{2\mu}{3}\right)\operatorname{tr} D\right]\right) \quad \text{during elastic response.}$$

Here, we have used the notation

$$(\Phi_S)_{ij} = \frac{\partial\phi}{\partial S_{ij}}$$

for the matrix of partial derivatives of the yield function with respect to the unrotated stress. During plastic loading, the stress lies on the yield surface, and the rates of deformation are such that elastic response would move the material state beyond the yield surface:

$$0 < \operatorname{tr}\left(\Phi_S\left[\Omega^T D\Omega 2\mu + I\left(\kappa - \frac{2\mu}{3}\right)\operatorname{tr} D\right]\right) \quad \text{during plastic loading.}$$

In order to determine the rates of plastic deformation during plastic loading, two pieces of information must be specified. First, we must specify the rate of change of the hardening parameter. Generally, this is taken to be a linear function of the unrotated rate of plastic deformation:

$$\frac{d\chi}{d\tau} = \operatorname{tr}(X_E \Omega^T D^p \Omega).$$

Secondly, a flow rule must be prescribed. We shall discuss associated flow rules, derived from Drucker's hypothesis, which basically states that useful net energy in addition to the elastic energy cannot be extracted from the material and the applied forces. Rather than formulate this hypothesis mathematically, let us list some of its conclusions. First, the yield surface must be a convex function of stress. Second, the plastic rate of deformation must be normal to the yield surface, pointing out of the region of admissible stresses, at points where the latter is continuously differentiable, and must lie between adjacent normals at points where the yield surface is not continuously differentiable. Third, the plastic rate of deformation must be a linear function of the stress rate. (A simple derivation of these conclusions appears in Fung [13]. For finite strains, the normality condition is not a necessary consequence of Drucker's postulate; see Naghdi and Trapp [33].)

Now we can derive a formula for the plastic rate of deformation from these conclusions of Drucker's hypothesis. At points where ϕ is continuously differentiable, the associated flow rule requires that the unrotated rate of plastic deformation satisfies

$$\Omega^T D^p \Omega = \Phi_S \alpha$$

for some positive scalar α. Thus during plastic loading,

$$0 = \frac{d\phi}{d\tau} = \operatorname{tr}\left(\Phi_S \frac{dS}{d\tau}\right) + \frac{\partial\phi}{\partial\chi}\operatorname{tr}(X_E \Omega^T D^p \Omega) = \operatorname{tr}\left(\Phi_S\left[\Omega^T D\Omega 2\mu + I\left(\kappa - \frac{2\mu}{3}\right)\operatorname{tr} D\right]\right)$$

$$+ \left\{\frac{\partial\phi}{\partial\chi}\operatorname{tr}(X_E \Phi_S) - \operatorname{tr}\left(\Phi_S\left[\Phi_S 2\mu + I\left(\kappa - \frac{2\mu}{3}\right)\operatorname{tr}\Phi_S\right]\right)\right\}\alpha.$$

We can solve this equation for α to get

$$\alpha = \frac{1}{\beta}\operatorname{tr}\left(\Phi_S\left[\Omega^T D\Omega 2\mu + I\left(\kappa - \frac{2\mu}{3}\right)\operatorname{tr} D\right]\right),$$

where

$$\beta = \operatorname{tr}\left(\Phi_S\left[\Phi_S 2\mu + I\left(\kappa - \frac{2\mu}{3}\right)\operatorname{tr}(\Phi_S) - \frac{\partial\phi}{\partial\chi} X_E\right]\right).$$

6.2.3. Acoustic Tensor

This equation allows us to write the stress rate in terms of the rate of deformation:

$$\Omega \frac{dS}{d\tau} \Omega^{\mathrm{T}} = D2\mu + I\left(\kappa - \frac{2\mu}{3}\right)\mathrm{tr}\, D - \left[\Omega\Phi_S\Omega^{\mathrm{T}}2\mu + I\left(\kappa - \frac{2\mu}{3}\right)\mathrm{tr}\,\Phi_S\right]\mathrm{tr}\left(\Phi_S\left[\Omega^{\mathrm{T}} D\Omega 2\mu + I\left(\kappa - \frac{2\mu}{3}\right)\mathrm{tr}\, D\right]\right)\frac{1}{\beta}.$$

Note that we can use the ordinary differential equation (6.9) for the rotation matrix Ω to rewrite this equation in the form

$$\frac{dS_{\mathrm{E}}}{d\tau} + \frac{1}{2}\left[\left(\frac{\partial \mathrm{v}}{\partial x}\right)^{\mathrm{T}} - \frac{\partial \mathrm{v}}{\partial x}\right]S_{\mathrm{E}} + S_{\mathrm{E}}\left[\frac{\partial \mathrm{v}}{\partial x} - \left(\frac{\partial \mathrm{v}}{\partial x}\right)^{\mathrm{T}}\right]\frac{1}{2} = \left[\frac{\partial \mathrm{v}}{\partial x} + \left(\frac{\partial \mathrm{v}}{\partial x}\right)^{\mathrm{T}}\right]\mu + I\left(\kappa - \frac{2\mu}{3}\right)\mathrm{tr}\frac{\partial \mathrm{v}}{\partial x} - \left[\Omega\Phi_S\Omega^{\mathrm{T}}2\mu + I\left(\kappa - \frac{2\mu}{3}\right)\mathrm{tr}\,\Phi_S\right]\frac{1}{\beta} \times \mathrm{tr}\left(\Phi_S\left[\Omega^{\mathrm{T}}\left\{\frac{\partial \mathrm{v}}{\partial x} + \left(\frac{\partial \mathrm{v}}{\partial x}\right)^{\mathrm{T}}\right\}\Omega\mu + I\left(\kappa - \frac{2\mu}{3}\right)\mathrm{tr}\frac{\partial \mathrm{v}}{\partial x}\right]\right).$$

In this way, we find that the acoustic tensor is

$$A_{\mathrm{E}} = H - m\frac{1}{\rho_{\mathrm{E}}\beta}m^{\mathrm{T}} + C, \tag{6.11}$$

where H and C are given by (6.8)-(6.9), and

$$m = \Omega\Phi_S\Omega^{\mathrm{T}} n_{\mathrm{E}} 2\mu + n_{\mathrm{E}}\left(\kappa - \frac{2\mu}{3}\right)\mathrm{tr}\,\Phi_S.$$

Again, we must perform some analysis to show that this matrix has real positive eigenvalues.

6.2.4. Analysis of Hyperbolicity

The eigenvalues of H are μ/ρ_{E}, μ/ρ_{E}, and $(\kappa + 4\mu/3)1/\rho_{\mathrm{E}}$. Standard estimates from linear algebra (see [15]) can be used to show that the eigenvalues λ_i of $H - m(1/\rho_{\mathrm{E}}\beta)m^{\mathrm{T}}$ satisfy

$$\frac{\mu}{\rho_{\mathrm{E}}} - \frac{m^{\mathrm{T}}m}{\rho_{\mathrm{E}}\beta} \leqq \lambda_1 \leqq \frac{\mu}{\rho_{\mathrm{E}}} = \lambda_2 \leqq \lambda_3^2 \leqq \frac{\kappa + \frac{4\mu}{3}}{\rho_{\mathrm{E}}}.$$

If we can ignore the contribution C to the acoustic tensor from the stress rate terms, then the characteristic speeds for the material undergoing plastic yield cannot be larger than the characteristic speeds during elastic response. We could also use the first inequality to determine a sufficient condition for hyperbolicity; however, we shall perform a different analysis to derive a necessary and sufficient condition.

Note that congruence relations preserve the signature of matrices; in other words, two congruent matrices have the same number of positive, zero, and negative eigenvalues. Our goal will be to use a congruence transformation to develop a necessary and sufficient condition for the positivity of $H - m(1/\rho_{\mathrm{E}}\beta)m^{\mathrm{T}}$. Let Q be the orthogonal matrix in (6.10). Then $H - m(1/\rho_{\mathrm{E}}\beta)m^{\mathrm{T}}$ is congruent to

$$H^{-1/2}Q^{\mathrm{T}}\left[I\frac{\mu}{\rho_{\mathrm{E}}} + n_{\mathrm{E}}\frac{\kappa + \frac{\mu}{3}}{\rho_{\mathrm{E}}}n_{\mathrm{E}}^{\mathrm{T}} - m\frac{1}{\rho_{\mathrm{E}}\beta}m^{\mathrm{T}}\right]QH^{-1/2} = I - H^{-1/2}Q^{\mathrm{T}}m(1/\rho_{\mathrm{E}}\beta)m^{\mathrm{T}}QH^{-1/2}.$$

Two of the eigenvalues of this matrix are one; the other eigenvalue is positive if and only if

$$1 > \frac{1}{\rho_{\mathrm{E}}\beta}m^{\mathrm{T}}QH^{-1}Q^{\mathrm{T}}m = \frac{1}{\mu\rho_{\mathrm{E}}\beta}m^{\mathrm{T}}Q\left[I - e_1\frac{\kappa + \frac{\mu}{3}}{\kappa + \frac{4\mu}{3}}e_1^{\mathrm{T}}\right]Q^{\mathrm{T}}m = \frac{1}{\mu\rho_{\mathrm{E}}\beta}\left[m^{\mathrm{T}}m - (m^{\mathrm{T}}n_{\mathrm{E}})^2\frac{\kappa + \frac{\mu}{3}}{\kappa + \frac{4\mu}{3}}\right]. \tag{6.12}$$

This gives us a necessary and sufficient condition for the positivity of the matrix $H - m(1/\rho_{\mathrm{E}}\beta)m^{\mathrm{T}}$.

6.2.5. Von Mises Yield Surface

As a special case, we consider the von Mises yield surface

$$\phi(S') = \tfrac{1}{2}\mathrm{tr}\, S'^2 - \eta^2,$$

where S' is the unrotated stress deviator

$$S' = S - I\frac{\mathrm{tr}\, S}{3}.$$

This is a perfectly plastic yield surface for which

$$\Phi_S = S' \quad , \quad X_{\mathrm{E}} = 0,$$

$$m = \Omega S'\Omega^{\mathrm{T}} n_{\mathrm{E}} 2\mu \quad , \quad \beta = 2\mu\,\mathrm{tr}\, S'^2 = 4\mu\eta^2.$$

Condition (6.12) for the positivity of the eigenvalues of $H - m(1/\rho_E \beta)m^T$ becomes

$$\tfrac{1}{2} \operatorname{tr} S'^2 > n_E^T \Omega S'^2 \Omega^T n_E - (n_E^T \Omega S' \Omega^T \eta_E)^2 \frac{\kappa + \frac{\mu}{3}}{\kappa + \frac{4\mu}{3}}$$

for all unit vectors n_E. Let us define

$$\tilde{S} = Q^T \Omega S' \Omega^T Q,$$

where Q is defined in (6.10). Then the inequality (6.12) is equivalent to

$$\tfrac{1}{2}\tilde{S}_{ij}\tilde{S}_{ij} = \tfrac{1}{2} \operatorname{tr} \tilde{S}^2 > e_1^T \tilde{S}^2 e_1 - (e_1^T \tilde{S} e_1)^2 \frac{\kappa + \frac{\mu}{3}}{\kappa + \frac{4\mu}{3}} = \tilde{S}_{1j}\tilde{S}_{1j} - \tilde{S}_{11}^2 \frac{\kappa + \frac{\mu}{3}}{\kappa + \frac{4\mu}{3}}.$$

After expanding the sums in this expression and canceling terms, we obtain the following necessary and sufficient condition (if we can ignore the contribution C of the terms from the stress rate in the acoustic tensor) for real characteristic speeds during plastic loading with a von Mises yield surface:

$$\tilde{S}_{22}^2 + \tilde{S}_{23}^2 + \tilde{S}_{32}^2 + \tilde{S}_{33}^2 + \tilde{S}_{11}^2 \frac{\kappa - \frac{2\mu}{3}}{\kappa + \frac{4\mu}{3}} > 0.$$

This inequality will be true if Poisson's ratio,

$$\frac{1}{2} \frac{\kappa - \frac{2\mu}{3}}{\kappa + \frac{\mu}{3}},$$

is non-negative. For most metals, Poisson's ratio is approximately 0.3, and the hyperbolicity of the equations of motion is closer to being established.

6.2.6. Nonsymmetric Stress Rate Terms

We have postponed until now the discussion of the effect of the matrix C on the eigenvalues of the acoustic tensor (6.11) for plastic loading. Since C, defined by (6.9), is linear in S_E and zero if S_E is a multiple of a diagonal matrix, it can only depend on the deviatoric stress S'. The yield function ϕ typically bounds the deviatoric stress, keeping its norm typically two orders of magnitude smaller than the shear modulus μ. Thus, C contributes only a small perturbation to the acoustic tensor, and will not destroy hyperbolicity of the equations of motion unless the eigenvalues of $H - m(1/\rho_E \beta)m^T$ are near zero or nearly equal.

We could try other stress rates that lead to symmetric acoustic tensors, such as the Truesdell stress rate, since reasonable thermodynamic assumptions require this symmetry. However, these stress rates lead to problems in numerical implementations, since zero stress rate does not imply constant invariants of stress. We would try hyperelastic models, since they do not involve the complications of objective stress rates, but they have not been successful in reproducing laboratory data. Our choice of models reflects the goal of our research: to study wave propagation in models of practical interest. The propagation of waves dominates our model requirements: the models must generate hyperbolic systems, so that initial-value problems are well posed. Given this caveat, we have shown that the models in this paper are acceptable for our numerical work below.

7. Numerical Method

Our next step is to describe a numerical method for solving the Lagrangian equations of motion. The basis of this method is to use the local hyperbolic structure of the equations of motion to upstream-center the differencing and to resolve the interaction of waves at cell interfaces. We acknowledge that there may be global pathologies in the wave structure that the current method may not be designed to handle. Our approach is to use this method to examine the structure of finite-amplitude waves, while proceeding with care due to the limitations of the numerical method.

We will use a second-order variant of Godunov's method, which is described in Colella and Glaz; see [10]. The reader interested in a survey of Godunov-type schemes for hyperbolic systems of conservation laws should read the paper by Harten *et al.* (see [18]); a recent survey of numerical methods for hyperbolic conservation laws can be found in Yee; see [50].

The second-order Godunov method has been very successful at computing the correct entropy-satisfying solutions to problems in gas dynamics, even in the presence of strong shocks. Lately, the second-order Godunov method has been applied to problems outside the realm of gas dynamics. The most notable of these applications has been petroleum reservoir simulation; see [4], [5], [42], [43]. This application involved considerable additional difficulties not present in gas dynamics, but found in solid mechanics. In reservoir simulation, the characteristic speeds are not necessarily hyperbolic, and they can be locally linearly degenerate. Furthermore, it is possible for the wavespeeds to be discontinuous at points where new fluid phases are formed. Because of the significantly greater complexity of the hyperbolic wave structure of the reservoir flow equations, it has been necessary to develop a stable and appropriately accurate approximate solution to the Riemann problem for general hyperbolic systems; see [6]. The success of the second-order Godunov

method on these very complicated problems gives some degree of confidence in extending this method to shocks in solids.

Since our numerical results in this paper will be restricted to one dimension, we shall restrict our review of the second-order Godunov method to one dimension, as well. The method consists of seven steps:

1. Characteristic analysis and time-step estimation;
2. Monotinized slope computation;
3. Characteristic tracing;
4. Flux computation;
5. Conservative differences;
6. Rotation update;
7. Stress update.

We shall consider each of these steps in turn.

7.1. Characteristic Analysis and Time-Step Estimation.

We compute the wavespeeds using the characteristic analysis applied to the non-conservation form (5.3) of the Lagrangian equations of motion. These equations involve derivatives of quantities

$$w = \begin{bmatrix} \mathbf{v} \\ \theta \\ S_E e_1 \end{bmatrix}$$

for problems in one dimension. We subscript w by its grid cell index, and superscript it by its discrete time level. With respect to these variables, we have shown in Section 5.1 how to compute the eigenvectors and eigenvalues of the linearized coefficient matrices. The maximum stable time step for the second-order Godunov method on a uniform grid is governed by the Courant-Friedrichs-Lewy condition

$$\lambda_{\max} \frac{\Delta\tau}{\Delta a} \leqq 1.$$

Here, $\lambda_{\max}$ is the largest absolute value of the eigenvalues of the linearized coefficient matrix B, as shown in (5.7). This condition must be satisfied for all the cells in the grid. Because the maximum wave speed of the continuum may not be sampled well in the discrete calculations, we usually require the left-hand side of this inequality to be less than 0.9.

7.2. Slope Computation

Our next step is to compute slopes in the flux variables w, to expand these slopes in terms of the characteristic directions, and to limit these characteristic expansion coefficients to preserve monotonicity. The effect of this is to selectively introduce numerical viscosity only in the individual cells and individual characteristic families that are attempting to oscillate. As a result, the amount of numerical viscosity added to the computation is greatly reduced.

We begin by using the eigenvectors from the characteristic analysis (5.7) to compute the vectors of expansion coefficients for the jumps in w:

$$X_j^k = \begin{bmatrix} X\Lambda & 0 & -X\Lambda \\ b_1^\dagger X & 1 & b_1^\dagger X \\ X\Lambda^2\rho_L & 0 & X\Lambda^2\rho_L \end{bmatrix},$$

$$c_{j+1/2} = (X_j^k)^{-1}(w_{j+1}^k - w_j^k)\frac{1}{\Delta a}, \tag{7.1}$$

$$c_j^c = (c_{j+1/2} + c_{j-1/2})^{1/2}.$$

Next, we modify these slopes in order to avoid the introduction of any new extrema in the piecewise-linear profile for the characteristic quantities. For the i-th wave family, the slope in the j-th cell at the k-th time level is given by

$$c_{ij}^k = \operatorname{sgn}(c_{ij}^c)\min\{\beta_{ij}|c_{i,j-1/2}|\ ,\ |c_{ij}^c|\ ,\ \beta_{ij}|c_{i,j+1/2}|\}, \tag{7.2}$$

where $\beta_{ij} \geqq 2$. For genuinely nonlinear conservation laws, it is permissible to take $\beta_{ij} = 2$. However, if the system of conservation laws possesses local linear degeneracies, it is sometimes necessary to take β_{ij} to be smaller; see [6]. In the examples of this paper, we found that $\beta_{ij} = 2$ was sufficient. However, in other applications to solid mechanics (see [44]) we have found it useful to compute β_{ij} as described in [2]: if differences between eigenvalues of the same family in neighboring cells indicate that the gradient of the characteristic speed has changed sign, then β is reduced to 1.5.

Also note that the characteristic speeds and directions can change abruptly when plastic loading begins or ends. These discontinuities in the characteristic structure are associated with shocks in the material response. In order to ensure that the computational scheme produces the correct discontinuities, we introduce additional numerical viscosity by setting $\beta_{ij} = 0$ in cells whose neighbors are not undergoing the same loading conditions.

7.3. Characteristic Tracing

The next step in the second-order Godunov method is to use the piecewise-linear profile described by (7.1) and (7.2) to approximate w at the cell edges and half-time level. From Taylor's theorem, the quasilinear form of the equations of motion (5.3), and the characteristic analysis we have

$$w(a_j + \tfrac{1}{2}\Delta a, \tau^k + \tfrac{1}{2}\Delta\tau) \approx w_j^k + \left(\frac{\partial w}{\partial a}\right)_j^k \tfrac{1}{2}\Delta a + \left(\frac{\partial w}{\partial \tau}\right)_j^k \tfrac{1}{2}\Delta\tau$$

$$= w_j^k + X_j^k[I\Delta a - \Lambda_j^k \Delta\tau]c_{j1/2}^k.$$

This approximation forms the edge-centered values of the flux variables by tracing the characteristics with positive characteristic speed into the j-th cell, and the characteristics with negative characteristic speed into the $(j+1)$-th cell. In order to use only upwind information in constructing the edge-centered states, we shall take

$$w^L_{j+1/2} = w^k_j + \sum_{i:\lambda_i>0} X^k_j e_i(\Delta a - \lambda^k_{ij}\Delta\tau)c^k_{ij+1/2}. \tag{7.3}$$

In a similar fashion, we trace

$$w^R_{j+1/2} = w^k_{j+1} - \sum_{i:\lambda_i<0} X^k_{j+1} e_i(\Delta a + \lambda^k_{ij}\Delta\tau)c^k_{ij+1/2}. \tag{7.4}$$

Even though these states ignore some of the terms needed to maintain second-order accuracy in the Taylor expansion, the solution of the Riemann problem in the next step will recover the accuracy.

7.4. Flux Computation

By tracing characteristics from the left and the right, we have used the piecewise-linear profiles to establish two distinct states at the cell edges. The interaction in time of these traced states can be resolved by solving a Riemann problem and evaluating the flux at the stationary state in its solution. Unfortunately, the analytic solution of the Riemann problems for the material models in this paper are not known; further, even if they were known, they would very likely be very complicated to evaluate. (See, for example, [25], [39], [41], and [46].)

Our approach is to approximate the solution of the Riemann problem. We note that the second-order Godunov method does not require that the local interactions of the waves be handled any more accurately than the underlying discretization errors. Our basic construction of the solution of the Riemann problem is motivated by the results of Wendroff in [48] and Liu in [29]. They showed that the left and right states in the Riemann problem are connected by a series of curves in state space corresponding to each of the characteristic families. It is well known that the eigenvectors are tangent to these wave curves for the appropriate families. This suggests that we expand the jump between the left and right states in terms of the eigenvectors. In one-dimensional Lagrangian coordinates, two or three of the characteristic speeds are positive, two or three are negative, and the remainder are zero. There are always two linearly independent characteristic directions corresponding to the zero wavespeeds; further, these directions are constant (since they are just columns of the identity matrix). If plastic yielding generates an additional pair of zero characteristic speeds, then there is only one linearly independent characteristic direction for this pair, with a corresponding eigenvector deficiency.

For simplicity, we shall ignore the eigenvector deficiency and reorder the eigenvalues and matrix X of eigenvectors

$$X^k_j = [(X^k_j)^+, X^0, (X^k_j)^-]$$

corresponding to the signs of the characteristic speeds. Next, we decompose the jump between the left and right states in terms of the eigenvectors from the upwind cells by solving for the expansion coefficients $c_{j+1/2}$ in

$$w^R_{j+1/2} - w^L_{j+1/2} = (X^k_j)^- c^-_{j+1/2} + X^0 c^0_{j+1/2} + (X^k_{j+1})^+ c^+_{j+1/2}.$$

We want to compute the flux at the intermediate state that moves with zero speed.

Since the information that moves with zero characteristic speed forms a contact discontinuity, its characteristic speed and its Rankine-Hugoniot speed should both be identical. Thus, it should be equivalent to use the flux evaluated at either

$$w^L_{j+1/2} + (X^k_j)^- c^-_{j+1/2}$$

or

$$w^R_{j+1/2} - (X^k_{j+1})^+ c^+_{j+1/2}.$$

We shall use the average of the flux at these two states to compute the approximate flux in our conservative difference scheme:

$$G^{k+1/2}_{j+1/2} = \tfrac{1}{2}[G_L(w^L_{j+1/2} + (X^k_j)^- c^-_{j+1/2}) + G_L(w^R_{j+1/2} - (X^k_{j+1})^+ c^+_{j+1/2})].$$

In the case that plastic yielding creates an eigenvector deficiency in one cell bordering the edge where we are computing the flux, then we use the existing characteristic direction for the degenerate zero speed to construct the approximate phase-space path. For example, if A_j is singular, we decompose the jump $w^R_{j+1/2} - w^L_{j+1/2}$ as before, and evaluate the flux at $w^L_{j+1/2}$ plus the sum of the parts of the approximate phase-space path corresponding to negative characteristic speeds (the part of the path corresponding to the degenerate zero speed is ignored). If both cells bordering the edge where the flux is being computed have eigenvector deficiencies, then we compute the least-squares projection of the jump onto the characteristic directions coming from nonzero wavespeeds, and continue with the flux evaluation as before. Because of rounding errors in the computations, the latter case is extremely rare.

7.5. Conservative Difference

The next step in the second-order Godunov method is to compute the conserved quantities at the new time level. By applying the divergence theorem to the conservation law (5.1)-(5.2) in the time-space box $|a - a_j| < \frac{1}{2}\Delta a$, $0 < \tau - \tau^k < \Delta\tau$, and by applying centered quadrature rules for the integrals, we obtain

$$u^{k+1}_j = u^k_j - \frac{\Delta\tau}{\Delta a}[G^{k+1/2}_{j+1/2} - G^{k+1/2}_{j-1/2}]. \tag{7.5}$$

Note that the characteristic tracing (7.2)-(7.3) was performed on the quasilinear form of the equations (5.3), while the conservative differences use the form (5.1)-(5.2). The quasilinear form incorporated the stress-rate equations directly, with the equality of mixed partials (1.3) used to replace time derivatives of the deformation gradient. However, the conservation form (5.1)-(5.2) used in the difference equation (7.5) gives us new values for the deformation gradient without updating the stress.

7.6. Rotation Update

For the Jaumann stress rate, we compute the rotation matrix by using the ordinary differential equation (6.3). This requires the spin tensor, which in turn depends on the velocity gradient. In order to compute the gradient of the velocity, we compute the current position vector x at the cell edges and half-time level by

$$x_{j+1/2}^{k+1/2} = x_{j+1/2}^{k} + v_{j+1/2}^{k+1/2}\Delta\tau\tfrac{1}{2}.$$

Here, the velocities were obtained by the solution of the Riemann problems at the cell edges. We compute the first column of the velocity gradient by

$$\left(\frac{\partial v}{\partial x}\right)_j^{k+1/2} = \frac{v_{j+1/2}^{k+1/2} - v_{j-1/2}^{k+1/2}}{x_{j+1/2}^{k+1/2} - x_{j-1/2}^{k+1/2}};$$

the second and third columns are zero since the motion is one-dimensional. The rate of deformation is taken to be the symmetric part D of the velocity gradient, and the spin tensor is the antisymmetric part.

Hughes in [20] and [22] shows how to integrate the ordinary differential equation (6.3) for the Jaumann rotation with second-order accuracy in time:

$$\Omega_j^{k+1} = \Omega_j^k + W_j^{k+1/2}[\Omega_j^{k+1} + \Omega_j^k]^{1/2}.$$

It is easy to see that Ω remains orthogonal:

$$\Omega_j^{k+1} = Q\Omega_j^k,$$

where the orthogonal matrix Q is defined by

$$Q = (I - W_j^{k+1/2}\tfrac{1}{2}\Delta\tau)^{-1}(I + W_j^{k+1/2}\tfrac{1}{2}\Delta\tau).$$

It is also useful to note that the spin tensor is singular, and its null vector z (which provides the axis of rotation for Q) satisfies

$$W_j^{k+1/2}b = z \times b \quad \text{for all vectors} \quad b.$$

This allows us to compute the square root of Q for use in evaluating the rotation tensor at the half-time level:

$$Q^{1/2} = (I - W_j^{k+1/2}\zeta)^{-1}(I + W_j^{k+1/2}\zeta),$$

where

$$\zeta = \frac{\tfrac{1}{2}\Delta\tau}{1 + \sqrt{1 + z^T z(\tfrac{1}{2}\Delta\tau)^2}}$$

7.7. Stress Update

The final step in our algorithm is to update the stress at the new time level. For an elastic or hyperelastic constitutive law, this requires only a direct evaluation. For constitutive laws specified by a stress-rate equation, it is necessary to integrate the ordinary differential equation (1.2) for the stress. This integration must be sufficiently accurate to maintain the global second-order spatial and temporal accuracy of the second-order Godunov method. Also, for plastic loading this ordinary differential equation needs to be integrated subject to the yield surface inequality $\phi \leqq 0$. Because the CFL condition for the conservative difference considers the rate of change of the stress, we shall not need to concern ourselves with the stability of our stress integration technique for large timesteps.

Because the constitutive laws are typically specified in terms of the Eulerian stress, we typically integrate (4.1) rather than (1.2). In order to compute a second-order accurate approximation to the stress at the new time level, we use an implicit trapezoidal method with a Lagrange multiplier correction for the yield condition; see [14]. This method takes the form

$$\frac{S_j^{k+1} - S_j^k}{\Delta\tau} e_i = \tfrac{1}{2}[\tilde{\mathbf{H}}_{i1}(S_j^k) + \tilde{\mathbf{H}}_{i1}(S_j^{k+1})]\left(\frac{\partial v}{\partial x_1}\right)_j^{k+1/2} e_i + \tfrac{1}{2}[\tilde{\mathbf{h}}_i(S_j^k) + \tilde{\mathbf{h}}_i(S_j^{k+1})]\frac{\theta_j^{k+1} - \theta_j^k}{\Delta\tau} + \Phi_s(S_j^{k+1})e_i\sigma.$$

Here, σ is a scalar chosen so that the yield condition $\phi = 0$ is satisfied exactly at the new time level. Note that the coefficients $\tilde{\mathbf{H}}_{ij}$, $\tilde{\mathbf{h}}_i$, and Φ_s have been evaluated at the half-time level by using averages of their values at the full-time levels. Since these coefficients can be nonlinear functions of the stress, the resulting difference method defines the stress at the new time level implicitly.

This does not necessarily mean that a nonlinear iteration is required to compute the new stress. Let us consider this method for a von Mises yield surface. If D' is the deviatoric part of the unrotated rate of deformation, then the rate equation for the unrotated stress deviator S' is

$$\frac{dS'}{d\tau} = D'2\mu - S'\frac{\operatorname{tr}(S'D')2\mu}{\operatorname{tr} S'^2}.$$

Using the implicit trapezoidal method, we obtain the discretization

$$\frac{S_j'^{k+1} - S_j'^{k}}{\Delta\tau} = D_j'^{k+1/2} 2\mu - \tfrac{1}{2}\left[S_j'^{k+1} \frac{\mathrm{tr}(S_j'^{k+1} D_j'^{k+1/2})}{\mathrm{tr}(S_j'^{k+1})^2} 2\mu + S_j'^{k} \frac{\mathrm{tr}(S_j'^{k} D_j'^{k+1/2})}{\mathrm{tr}(S_j'^{k})^2} 2\mu \right] + S_j'^{k+1}\sigma.$$

This gives us the equation

$$S_j'^{k+1}\left[1 + \frac{\Delta\tau}{2} \frac{\mathrm{tr}(S_j'^{k+1} D_j'^{k+1/2})}{\mathrm{tr}(S_j'^{k+1})^2} 2\mu - \sigma\Delta\tau \right] = S_j'^{k}\left[1 - \frac{\Delta\tau}{2} \frac{\mathrm{tr}(S_j'^{k} D_j'^{k+1/2})}{\mathrm{tr}(S_j'^{k})^2} 2\mu \right] + D_j'^{k+1/2} 2\mu\Delta\tau.$$

Thus, $S_j'^{k+1}$ is a scalar multiple of the matrix on the right. This suggests that we compute the matrix on the right, then compute the norm of the updated stress and scale the stress back to the yield surface. (However, for yield surfaces more complicated than von Mises, we have found it useful to use an implicit midpoint method; see [44].)

In order to compute the Eulerian stress at the new time level and cell center using the Jaumann stress rate, we must compute the unrotated stress at the old time level and the unrotated rate of deformation at the half-time level. The former is

$$S_j^k = (\Omega_j^k)^{\mathrm{T}} (S_{\mathrm{E}})_j^k \Omega_j^k,$$

while the latter is

$$(\Omega_j^k)^{\mathrm{T}} (Q^{1/2})^{\mathrm{T}} D_j^{k+1/2} Q^{1/2} \Omega_j^k.$$

After we have updated the unrotated stress, we need to rotate it to form the Eulerian stress at the new time level:

$$(S_{\mathrm{E}})_j^{k+1} = Q\Omega_j^k S_j'^{k+1} (\Omega_j^k)^{\mathrm{T}} Q^{\mathrm{T}}.$$

We also complete the computation of x at the new time level.

8. Numerical Results

We shall present several numerical results to illustrate the analysis of the characteristic structure for elastic-plastic solids and to demonstrate the success of the numerical method. All of our Cartesian examples are similar to, or modifications

of, problems due to Wilkins; see [49]. This model uses a von Mises yield surface to describe aluminum, for which the density, shear modulus, and yield strength are given by

$$\rho_{\mathrm{L}} = 2700 \text{ kg./m.}^3$$

$$\mu = 2.48 \times 10^{10} \text{ pa.}$$

$$\eta = 1.72 \times 10^{8} \text{ pa.}$$

The pressure is taken to be a function of the strain measure

$$\psi = \frac{1}{|F|} - 1 = \frac{\rho_{\mathrm{E}}}{\rho_{\mathrm{L}}} - 1;$$

specifically, the pressure is the following function of ψ in units of pascals:

$$p = \psi(7.3 \times 10^{10} + \psi(1.72 \times 10^{11} + \psi 4 \times 10^{10})).$$

From this, we compute the instantaneous bulk modulus

$$\kappa = \frac{\partial p}{\partial \psi} \frac{1}{|F|}.$$

In the calculations below, the Jaumann stress rate was used to describe the deviatoric behavior of the material.

In our first example, shown in Figures 1 and 2, we examine the results of one aluminum plate striking another at a velocity of 200 meters per second. Initially, the left plate hits the right plate in the center of the grid. The impact generates two waves moving left and two waves moving right. By plotting the variables versus the distance from the point of impact divided by the elapsed time, we readily see that both waves moving to the right are in the fast wave family. The fastest wave is a shock, called the elastic precursor. Because the yield condition creates a discontinuous change in the characteristic speeds, the elastic precursor is separated by a constant state from the slower shock, the plastic compressional wave. Note that the constant state separating these waves shows a discontinuous change in the characteristic speed, corresponding to the choice between during loading and unloading for states on the yield surface. In this problem, the volumetric strains (measured as the logarithm of the determinant of the deformation gradient) are small (less than 2%). Note that the numerically chosen characteristic speeds assume a very large value in the center of the grid. Due to computational errors, these states have fallen just inside the yield surface, and have adopted elastic characteristic speeds. The results in Figure 1 were obtained by using 500 cells in the grid. Figure 2 shows the pressure profile for calculations using 63, 125, 250, and 500 grid cells.

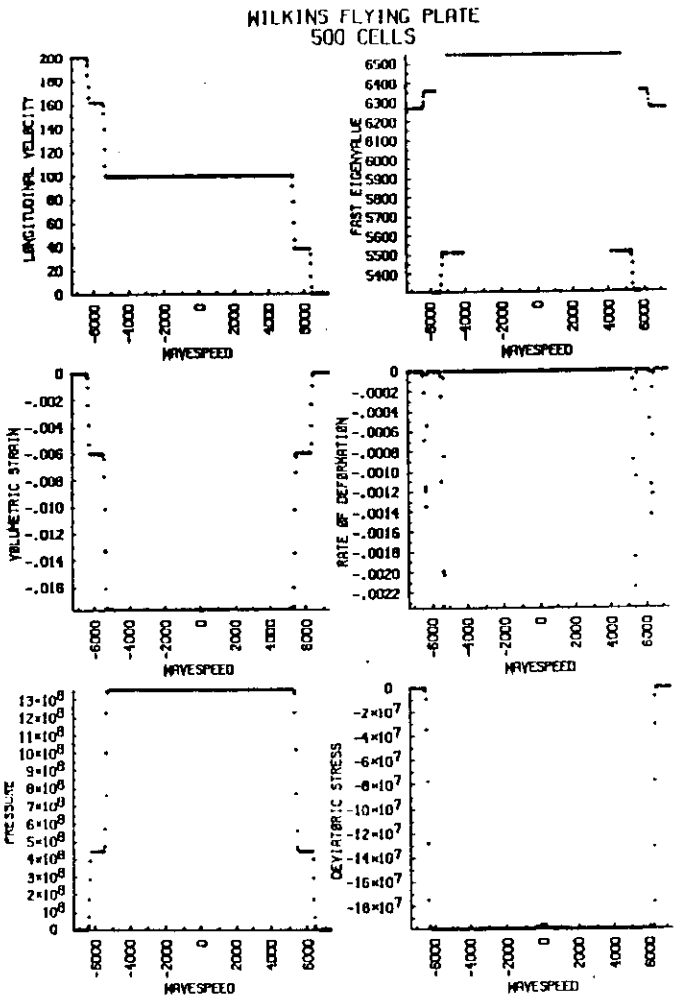

Figure 1. Infinite aluminum plates striking at 200 m/sec.

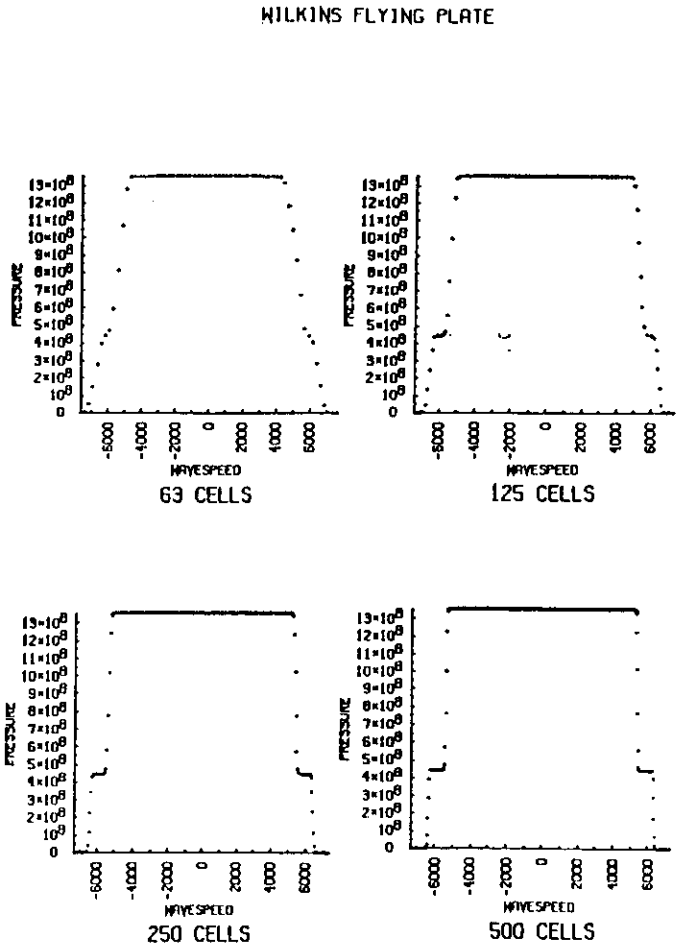

Figure 2. Grid refinement study for Figure 1.

In Figures 3 and 4 we show two plates striking at 2000 meters per second. In this problem, the elastic precursor is very small. However, the volumetric strains become quite large; and because the metal is so compressed in the constant state around the point of impact, the characteristic speeds reach large values in this

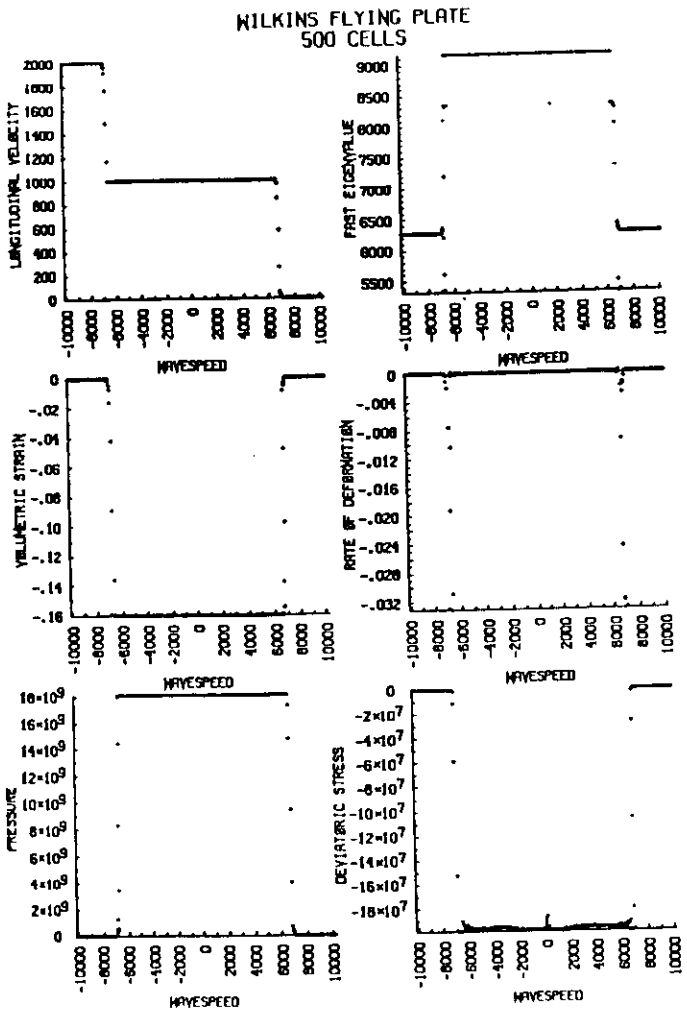

Figure 3. Infinite aluminum plates striking at 2000 m/sec.

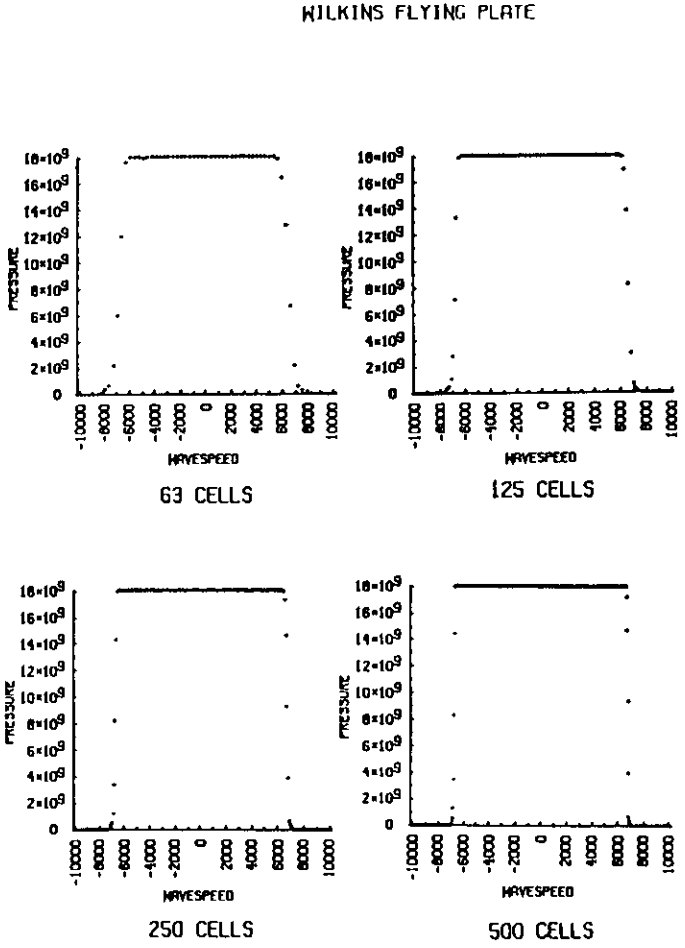

Figure 4. Grid refinement study for Figure 3.

plastic region. The plastic characteristic speed is around 8400 meters per second, but most of the cells contain elastic states near the yield surface with characteristic speeds around 9100 meters per second. Because of the strong compression, the plastic shock is very strong and self-steepening; as a result, a first-order method is

perfectly adequate for this problem. In fact, a pure second-order version of Godunov's method produces shocks that are too sharp and oscillate behind the wave. We have used slope flattening (see [9]) to introduce a linear viscosity in those cells that are in the midst of strong shocks. Figure 4 shows the results of a grid refinement study for this problem.

In Figures 5 and 6 we show the total stress (first diagonal entry of the Cauchy stress tensor) in a one-centimeter wide aluminum plate striking a four-centimeter wide plate. The impact velocity in Figure 5 is 800 meters per second, and 2000 meters per second in Figure 6. Initially, the impact generates an elastic precursor and a plastic wave in pairs moving left and right. As the waves moving left bounce off the free surface, they become rarefactions moving right and overtake the shocks moving to the right. In contrast to the results in [49], the elastic precursor shock is very well resolved in Figure 5, and there are no noticeable oscillations behind the slow rarefaction.

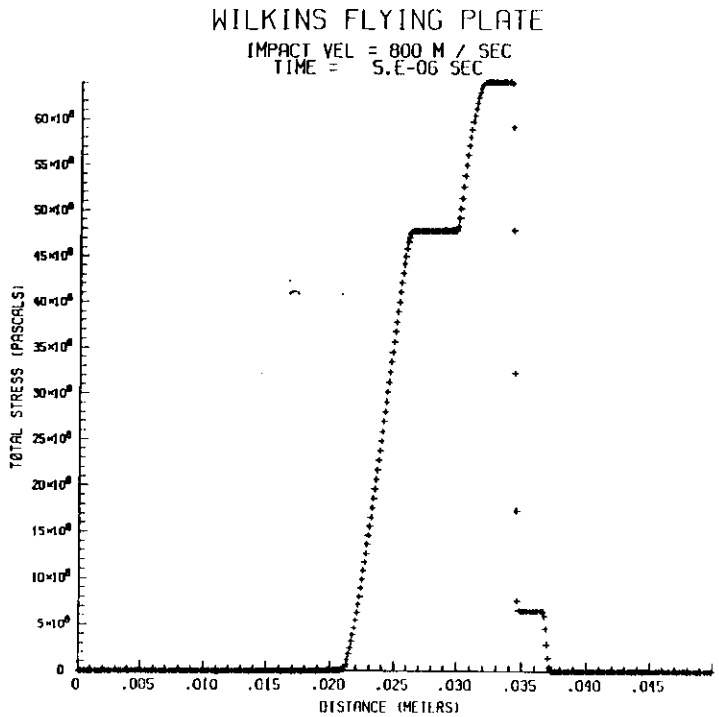

Figure 5. Finite aluminum plates striking at 800 m/sec.

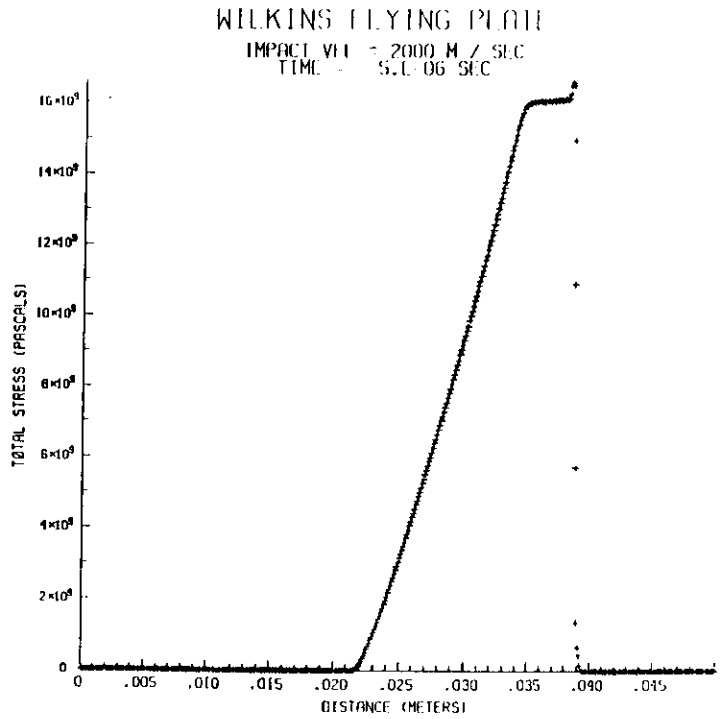

Figure 6. Finite aluminum plates striking at 2000 m/sec.

In Figures 7 and 8, we impulsively stretched an aluminum plate by giving the left half a velocity of 200 meters per second. In this case, elastic precursor and plastic waves are both rarefactions, as is clearly indicated by the plot of the eigenvalue. Normally, the metal would have been modeled as reaching failure when the pressure reached minus one-third the yield strength; however, we suppressed the failure model in this calculation. Also note that the constant state between the elastic precursor and the plastic wave has a discontinuous change in its characteristic speed, due to a change in the direction of loading at a state on the yield surface. Figure 8 shows a grid refinement study for this problem.

In Figure 9 we show the results of shearing an aluminum plate with a transverse velocity of 10 meters per second. This generates a relatively large elastic shear wave moving at slightly more than 3000 meters per second; the eigenvalue plots identify this wave as a weak shock. The shearing motion also generates a small compressional

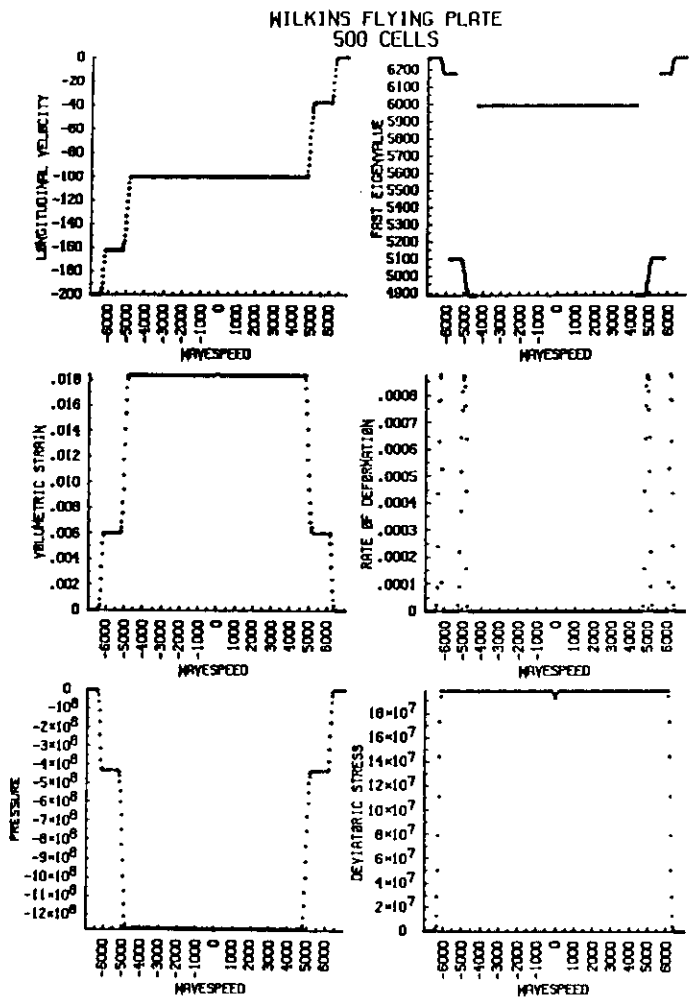

Figure 7. Infinite aluminum plate stretched at 200 m/sec.

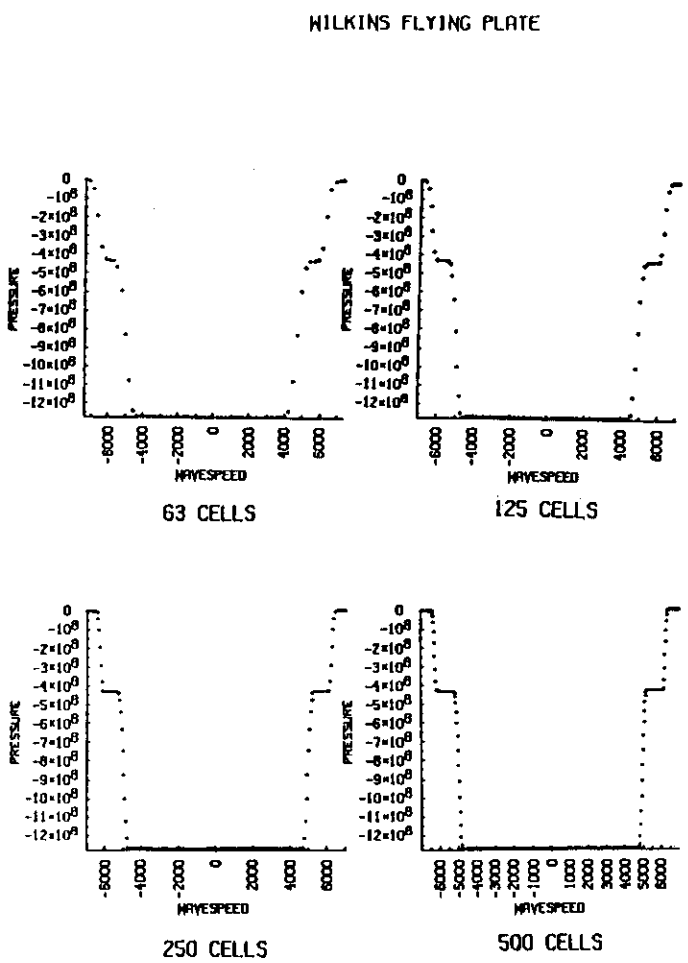

Figure 8. Grid refinement study for Figure 7.

wave, moving at more than 6000 meters per second; this wave is also a shock. The longitudinal velocity in this wave (Figure 9a) is four orders of magnitude smaller than the transverse velocity that initiated the motion, and appears from grid refinement studies to be correctly resolved in this figure. Figure 9b shows that the

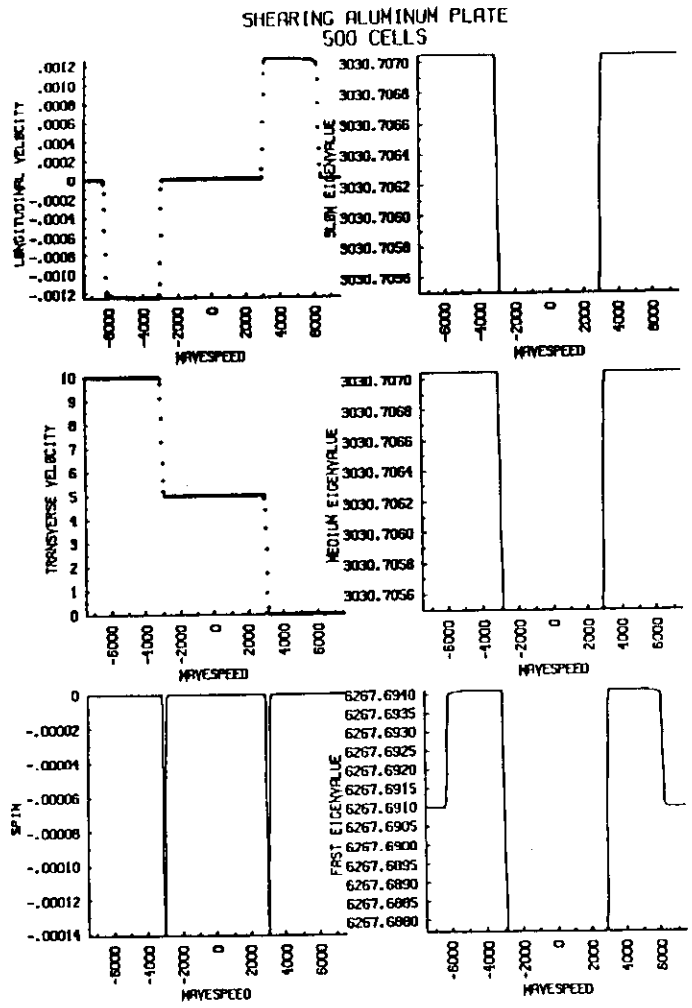

Figure 9. Infinite aluminum plate sheared at 10 m/sec. (a) Velocities and characteristic speeds.

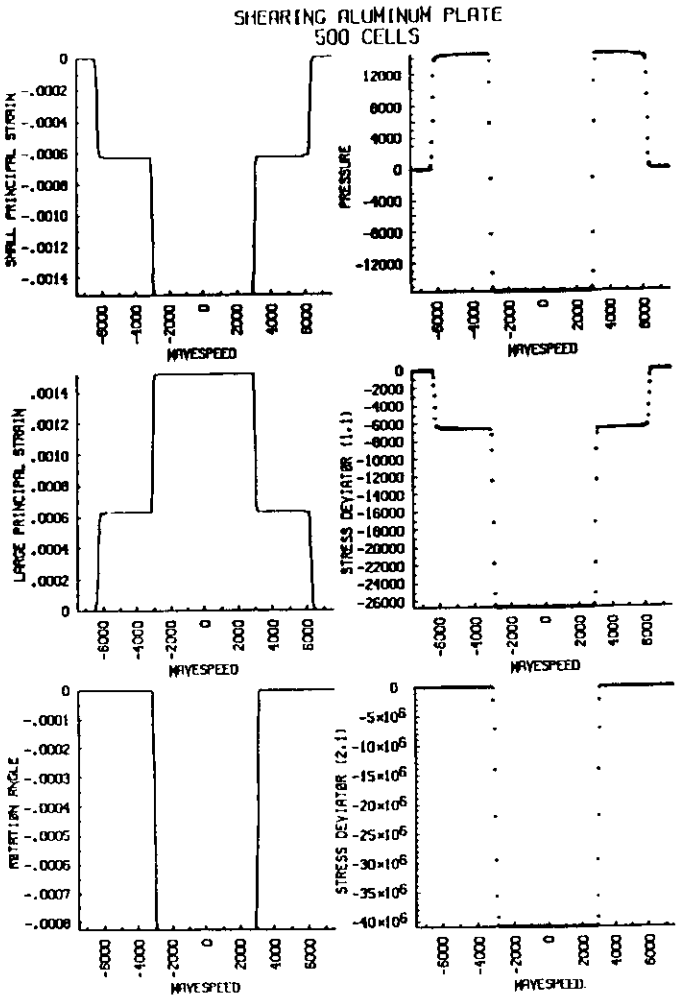

Figure 9. Infinite aluminum plate sheared at 10 m/sec. (b) Stresses and strains.

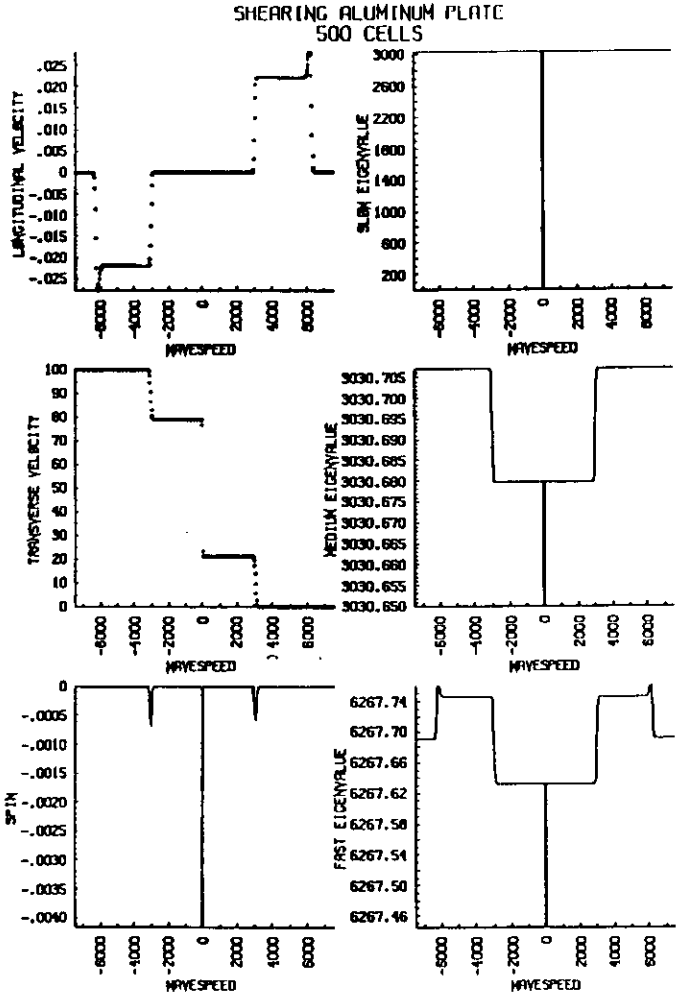

Figure 10. Infinite aluminum plate sheared at 100 m/sec. (a) Velocities and characteristic speeds.

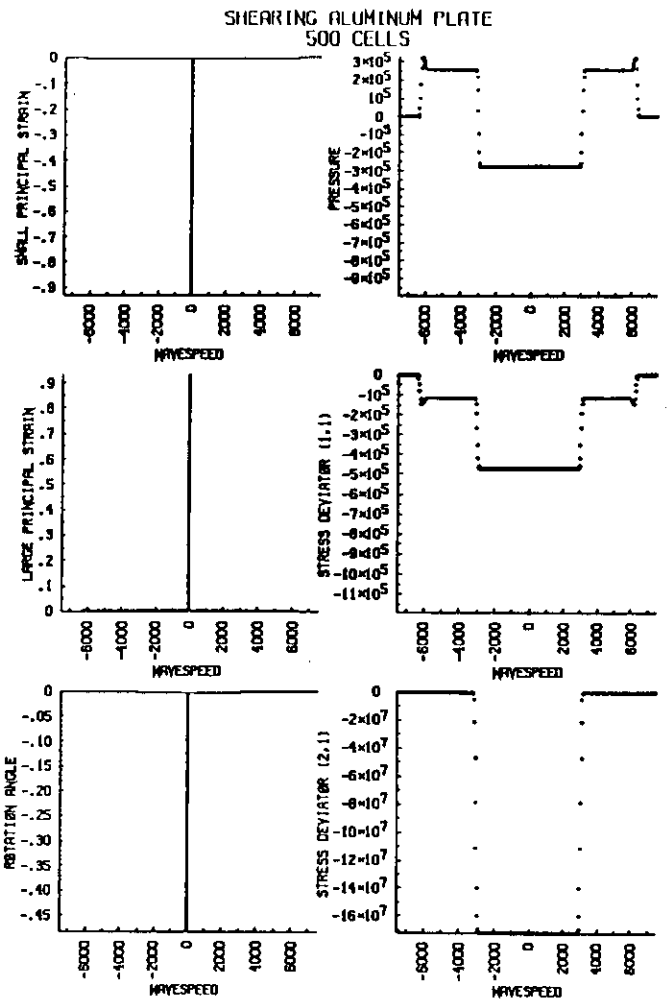

Figure 10. Infinite aluminum plate sheared at 100 m/sec. (b) Stresses and strains.

strains are very small, and the maximum rotation in the polar decomposition of the deformation gradient is also very small.

In Figure 10 we shear the plate with a transverse velocity of 100 meters per second. In this case, the material yields in the center, and the smallest characteristic speed is zero at this point. This corresponds to an eigenvector deficiency in the characteristic structure (see Section 5 above). There is a compound fast wave, involving a rarefaction and a shock, moving at more than 6000 meters per second. This wave generates longitudinal velocities that are roughly four orders of magnitude smaller than the transverse velocities. There is also an elastic shear wave, moving at slightly more than 3000 meters per second. The stationary wave is due to plastic yielding, and would normally correspond to failure of the material. Note that the material is highly rotated at the center, and that the principal strains (the logarithms of the eigenvalues of the symmetric matrix in the polar decomposition of the deformation gradient) are very large at the center.

Our next set of examples involves a spherically symmetric elastic material undergoing infinitesimal displacements. Although this problem does not exercise the large displacement aspects of our numerical method, nor the plasticity models, it does generate interesting results for which there are analytic solutions due to Blake; see [7]. We have made minor modifications to the second-order Godunov method in order to handle the spherical symmetry. The characteristic analysis of the models is easily incorporated, but the geometric source terms must be accounted in the characteristic tracing step and the conservative update.

Our material has an elastic modulus

$$E = 6 \times 10^{10} \text{ pa.}$$

and a Poisson ratio of 0.2702. This leads to the following bulk and shear moduli:

$$\kappa = 4.35 \times 10^{10} \text{ pa.}$$

$$\mu = 2.36 \times 10^{10} \text{ pa.}$$

The material density is

$$\rho_L = 3000 \text{ kg/m}^3.$$

At the inner radius of 0.1 meters we impose a constant pressure of 10^6 pascals for $t > 0$.

Figures 11 and 12 show a comparison between the numerical solution with the second-order Godunov method and the analytic solution due to Blake. Blake's solution is plotted with a solid line, and the cell-centered values of the numerical solution are plotted with + signs. In Figure 11 we show the profile of the radial displacement, velocity, θ, θ component of the deviatoric stress, and the pressure at 1.6×10^{-4} seconds, for a 200 cell grid. Note that the peak velocity and pressure

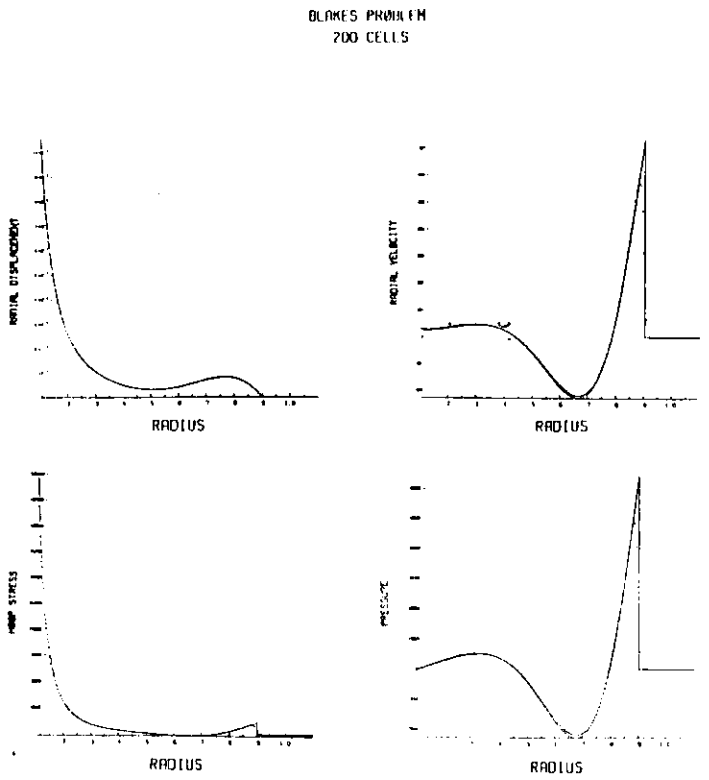

Figure 11. Solutions profiles for Blake's problem.

are less than the analytic values; also note that the Godunov method is placing about five cells in the discontinuity. This is the case because the discontinuity is very weak, since the nonlinearities in the model are not active. (The radial displacement at the inner radius is six orders of magnitude smaller than the radial position, so the volumetric strains are truly infinitesimal.) In Figure 12 we show the results of a grid refinement study for the pressure. These results show linear convergence of the peak pressure to its analytic value, due to the errors in capturing the discontinuity. Nevertheless, the results at all cell sizes are free of numerical oscillation and show convergence of the method to the correct answer.

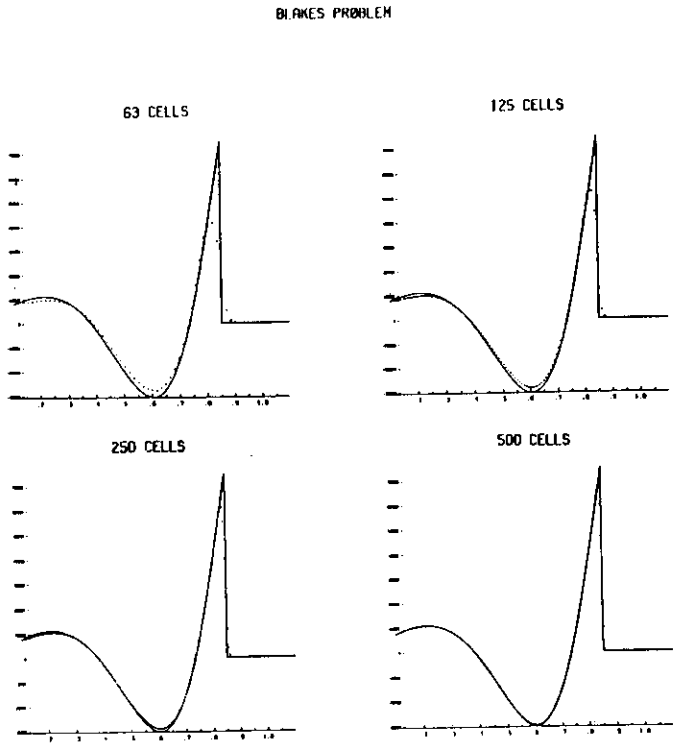

Figure 12. Grid refinement study for Blake's problem.

9. Conclusions

In this paper we have presented a complete set of equations needed to write the equations of motion for finite deformation of solids in first-order conservation form, in both the Lagrangian and Eulerian frames of reference. We also examined the characteristic structure of these systems of equations in both frames of reference, including thermal effects, in order to determine the circumstances under which the characteristic speeds are real and to guarantee the correct relationship between the two sets of characteristic speeds. We analyzed several models of common usage and showed that both elastic and plastic response with these models leads to hyperbolic systems, under reasonable conditions on the model parameters. We found the possibility of coincident wavespeeds, eigenvector deficiencies, compound waves due to local linear degeneracies, discontinuous change in the characteristic structure at yield, and multiple waves in the same characteristic family separated by constant states. Finally, we constructed a second-order Godunov method that successfully solved a variety of problems in one Lagrangian coordinate dimension, without introducing annoying numerical oscillations or algorithmic parameters that require fine tuning. Our numerical method was able to resolve global pathologies in the wave structure, such as local linear degeneracies and nearly coalescing characteristic speeds, using only information about the local wave structure.

Two of these results are non-classical. First, we have studied the hyperbolicity of the equations of motion using a kinetic equation of state in rate-form. Second, we have studied the curl condition on the deformation gradient as a constraint on the first-order system of conservation laws. This constraint is similar to the div $B = 0$ condition in magneto-hydrodynamics, and must be periodically re-enforced in order to avoid problems in numerical schemes.

In forthcoming papers, we shall describe the extension of the second-order Godunov method to problems in multiple spatial dimensions. We have also applied the method to more complicated material models; indeed, we have already completed a numerical implementation of a second-order Godunov method for the cap model; see [44]. In a parallel effort, we have examined the structure of finite-amplitude waves in the longitudinal motion of one-dimensional nonlinear solids with plastic yielding; see [45]. However, the extension of analytic techniques to the solution of Riemann problems for systems of more than two equations is, in general, very difficult.

We acknowledge that there may be global pathologies in the wave structure that the current method may not be designed to handle. Our approach is to use this method to examine the structure of finite-amplitude waves, while proceeding with care due to the limitations of the numerical method. We have, however, observed local linear degeneracies, as well as nearly coincident wavespeeds which should have corresponding eigenvector deficiencies. These pathological waves are shown in Figure 10, and have been captured adequately using the method described in this paper.

This work has raised several interesting mathematical questions. For example, it is not clear that the jumps obtained at discontinuities must be independent of the path of integration for the ordinary differential equations describing the kinetic equation of state. In our calculations thus far, we have not observed any indications of any sensitivities in this regard; if they exist, these phenomena could be activated by changes in the CFL timestep selection parameter. It is also unknown if correct jumps occur in the limit of vanishing diffusion or dispersion.

We also note that this work raises some questions about the correct formulation of material models. Because of the asymmetry of the acoustic tensor for the Jaumann or Green-Naghdi stress rates, it is possible that complex wavespeeds might be obtained in some circumstances.

Acknowledgments. A number of people have helped us with the finer points of finite deformations and plasticity in solids. At Lawrence Livermore National Laboratory, we have benefitted greatly from discussions with Ray Stout and Lewis Thigpen on the equations of motion, and with Gerry Goudreau and Brad Maker on computational methods. Linda Petzold has been very helpful in discussions on differential algebraic equations. We would also like to acknowledge several useful discussions with Stu Antman of the University of Maryland. However, our most sincere gratitude is extended to Tom Hughes of Stanford, for his comments on earlier drafts of this manuscript, particularly with regard to constitutive models.

This work was performed, in part, under the auspices of the U.S. Department of Energy by the Lawrence Livermore National Laboratory under contract No. W-7405-Eng-48. Partial support under contract No. W-7405-Eng-48 was provided by the Applied Mathematical Sciences Program of the Office of Energy Research, and by the Defense Nuclear Agency.

Bibliography

[1] Eringen, A. C., and Suhubi, E. S., *Elasto-Dynamics, Vol. I, Finite Motions*, Academic Press, 1974.
[2] Allen, M. B., III, Behie, G. A., and Trangenstein, J. A., *Multi-Phase Flow in Porous Media: Mechanics, Mathematics and Numerics*, Lecture Notes in Engineering 34, Springer-Verlag, 1988.
[3] Bazant, Z. P., *A correlation study of formulations of incremental deformation and stability of continuous bodies*, J. Appl. Mech. 38, 1971, pp. 919–928.
[4] Bell, J. B., Shubin, G. R., and Trangenstein, J. A., *A method for reducing numerical dispersion in two-phase black-oil reservoir simulation*, J. Comp. Phys. 65, 1986, pp. 71–106.
[5] Bell, J. B., Dawson, C. N., and Shubin, G. R., *An unsplit, higher-order Godunov method for scalar conservation laws in multiple dimensions*, J. Comp. Phys. 74, 1988, pp. 1–24.
[6] Bell, J. B., Colella, P., and Trangenstein, J. A., *Higher-order Godunov methods for general systems of hyperbolic conservation laws*, J. Comp. Phys. 82, 1989, pp. 362–397.
[7] Blake, F. G., *Spherical wave propagation in solid media*, J. Acous. Sci. Amer. 24, 1952, pp. 211–215.
[8] Boris, J. P., and Book, D. L., *Flux corrected transport III: minimal error FCT algorithms*, J. Comp. Phys. 20, 1976, pp. 397–431.
[9] Colella, P., and Woodward, P., *The piecewise parabolic method (PPM) for gas-dynamical simulations*, J. Comp. Phys. 54, 1984, pp. 174–201.
[10] Colella, P., and Glaz, H. M., *Efficient solution algorithms for the Riemann problem for real gases*, J. Comp. Phys. 59, 1985, pp. 264–289.
[11] Cristescu, N., *Dynamic Plasticity*, North-Holland, 1967.
[12] Frederick, D., and Chang, T. S., *Continuum Mechanics*, Allyn and Bacon, 1965.
[13] Fung, Y. C., *Foundations of Solid Mechanics*, Prentice-Hall, 1965.
[14] Gear, C. W., *Maintaining solution invariants in the numerical solution of ODEs*, SIAM J. Sci. Stat. Comput. 3, 1986, pp. 734–743.
[15] Golub, G. H., and van Loan, C. F., *Matrix Computations*, Johns Hopkins, 1983.
[16] Green, A. E., and Naghdi, P. M., *A general theory of an elastic-plastic continuum*, Arch. Rat. Mech. Anal. 18, 1965, pp. 251–281.
[17] Hanyga, A., *Mathematical Theory of Non-Linear Elasticity*, Ellis Horwood, 1985.
[18] Harten, A., Lax, P. D., and van Leer, B., *On upstream differencing and Godunov-type schemes for hyperbolic conservation laws*, SIAM Rev. 25, 1983, pp. 35–61.
[19] Holden, H., *On the Riemann problem for a prototype of a mixed type conservation law*, Comm. Pure Appl. Math. 40, 1987, pp. 229–264.

[20] Hughes, T. J. R., and Winget, J., *Finite rotation effects in numerical integration of rate constitutive equations arising in large-deformation analysis*, Internat. J. Numer. Meth. Eng. 15, 1980, pp. 1862–1867.
[21] Hughes, T. J. R., and Brooks, A., *A theoretical framework for Petrov-Galerkin methods with discontinuous weighting functions: Application to the streamline-upwind procedure*, in *Finite Elements in Fluids* 4, Wiley, 1982, pp. 47–65.
[22] Hughes, T. J. R., *Numerical implementation of constitutive models: rate-independent deviatoric plasticity*, in *Mechanics of Elastic and Inelastic Solids* 6, Martinus Nijhoff, 1984, pp. 29–63.
[23] Johnson, C., and Saranen, J., *Streamline diffusion methods for the incompressible Euler and Navier-Stokes equations*, Math. Comp. 47, 1986, pp. 1–18.
[24] Johnson, G. C., and Bammann, D. J., *A discussion of stress rates in finite deformation problems*, Int. J. Solids Struc. 20, 1984, pp. 725–737.
[25] Keyfitz, B. L., and Kranzer, H. C., *A system of nonstrictly hyperbolic conservation laws arising in elasticity theory*, Arch. Rat. Mech. Anal. 772, 1980, pp. 220–241.
[26] Kleiber, M., *Kinematics of deformation processes in materials subjected to finite elastic-plastic strains*, Int. J. Eng. Sci. 13, 1975, pp. 513–525.
[27] Kosinski, W., *Field Singularities and Wave Analysis in Continuum Mechanics*, Ellis Horwood, 1986.
[28] Lee, E. H., and Liu, D. T., *Finite-strain elastic-plastic theory with application to plane-wave analysis*, J. Appl. Phys. 38, 1967, pp. 19–27.
[29] Liu, T. P., *The Riemann problem for general systems of conservation laws*, J. Diff. Eqn. 18, 1975, pp. 218–234.
[30] Malvern, L. E., *Introduction to the Mechanics of a Continuous Medium*, Prentice-Hall, 1969.
[31] Mandel, J., *Ondes plastiques dans un milieu indéfini à trois dimensions*, J. de Méc. 1, 1962, pp. 3–30.
[32] Meeking, R. M., and Rice, J. R., *Finite element formulations for problems of large elastic-plastic deformation*, Int. J. Solids Struc. 11, 1975, pp. 601–616.
[33] Mehrabadi, M. M., and Nemat-Nasser, S., *Some basic kinematical relations for finite deformations of continua*, Mech. Mat. 6, 1987, pp. 127–138.
[34] Naghdi, P. M., and Trapp, J. A., *Restrictions on constitutive equations of finitely deformed elastic-plastic materials*, Q. J. Mech. Appl. Math. 28, 1975, p. 25.
[35] Nagtegaal, J. C., and de Jong, J. E., *Some aspects of nonisotropic work-hardening in finite deformation plasticity*, in *Proceedings of the Workshop on Plasticity of Metals at Finite Strain: Theory, Computation and Experiment*, E. H. Lee and R. L. Mallett, eds., Stanford University, 1981.
[36] Pinsky, P. M., Ortiz, M., and Pister, K. S., *Numerical integration of rate constitutive equations in finite deformation analysis*, Comp. Meth. Appl. Mech. Eng. 40, 1983, pp. 137–158.
[37] Plohr, B. J., and Sharp, D. H., *A conservative Eulerian formulation of the equations for elastic flow*, Adv. Appl. Math. 9, 1988, pp. 481–499.
[38] Prager, W., *An elementary discussion of definitions of stress rate*, Q. Appl. Math. 18, 1961, pp. 403–407.
[39] Schaeffer, D. G., and Shearer, M., *The classification of 2 × 2 systems of non-strictly hyperbolic conservation laws, with application to oil recovery*, Comm. Pure Appl. Math. 41, 1987, pp. 141–178.
[40] Shearer, M., *The Riemann problem for a class of conservation laws of mixed type*, J. Diff. Eqn. 46, 1982, pp. 426–445.
[41] Simo, J. C., and Ortiz, M., *A unified approach to finite deformation elastoplastic analysis based on the use of hyperelastic constitutive equations*, Comp. Meth. Appl. Mech. Eng. 49, 1985, pp. 221–245.
[42] Tang, Z., and Ting, T. C. T., *Wave curves for the Riemann problem of plane waves in isotropic elastic solids*, Int. J. Eng. Sci. 25, 1987, pp. 1343–1381.
[43] Trangenstein, J. A., and Bell, J. B., *Mathematical structure of the black-oil model for petroleum reservoir simulation*, SIAM J. Appl. Math. 49, 1989, pp. 749–783.
[44] Trangenstein, J. A., and Bell, J. B., *Mathematical structure of compositional reservoir simulation*, SIAM J. Sci. Stat. Comput. 10, 1989, pp. 817–845.